Coordination Chemistry Reviews 252 (2008) 2424–2443

Contents lists available at ScienceDirect

Coordination Chemistry Reviews

journal homepage: www.elsevier.com/locate/ccr

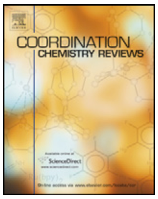

Review

Metal containing nanosized systems for MR-Molecular Imaging applications

Daniela Delli Castelli, Eliana Gianolio, Simonetta Geninatti Crich, Enzo Terreno, Silvio Aime*

Department of Chemistry IFM and Molecular Imaging Center, University of Torino, Via Nizza, 52, I-10126 Torino, Italy

ARTICLE INFO

Article history:
Received 23 January 2008
Accepted 14 May 2008
Available online 21 May 2008

Keywords:
Nanosized systems
Nanocarriers
Magnetic particles
MRI contrast agents
Molecular Imaging probes

ABSTRACT

This review aims at assessing the role of nanosized systems as MR-imaging reporters in Molecular Imaging applications.

The possibility of delivering a high number of imaging agents at the target of interest appears the solution of choice to overcome the drawback associated with the low sensitivity of the MRI approach. The use of metal-based particles entered very early in the armoury of MRI contrast agents with the Superparamagnetic Iron Oxides' family that are still among the most sensitive systems. The review devotes much attention to the design and use of self-assembled systems based on lipophilic molecules, reporting examples taken by products and processes developed in the authors' laboratory. The imaging reporters are invariantly represented by highly stable lanthanide(III) complexes. In general, whether is the paramagnetic lanthanide(III) ion, the particles act as T_2-susceptibility agents, whose contrasting abilities increase by increasing the magnetic field strength. In the case of Gd(III)-complexes, the systems mainly act as T_1-relaxation agents, whose efficiency is eventually enhanced by the long reorientational time of the supramolecular aggregate. In addition to tackle sensitivity issues, such systems may also be designed in order to become responsive to a specific physical or biochemical parameter of the microenvironment in which they distribute. Moreover, nanosized carriers for Gd(III)-complexes based on naturally occurring systems (apoferritin and lipoproteins) have also been considered for targeting specific epitopes on diseased cells.

Finally, liposomes have been exploited to generate a novel class of highly sensitive CEST (Chemical Exchange Saturation Transfer) agents dubbed LIPOCEST. Such systems are characterized by a shifted resonance for the large pool of water molecules entrapped in the liposomal cavity that can be selectively irradiated in order to transfer saturated magnetization to the bulk water signal.

Contents

---

* Corresponding author. Tel.: +39 011 6706451; fax: +39 011 6706477.
E-mail address: silvio.aime@unito.it (S. Aime).

0010-8545/$ – see front matter © 2008 Elsevier B.V. All rights reserved.
doi:10.1016/j.ccr.2008.05.006

1. Introduction

Molecular Imaging aims at the *in vivo* quantitative visualization of molecules and molecular events that occur at cellular level [1]. The potential towards clinical translation is huge as the same modalities used in Medical Imaging are used in Molecular Imaging investigations. Traditionally, Medical Imaging was a tool for non-invasive mapping of anatomy and for the detection of and localization of a disease process. The advent of Molecular Imaging based protocols will allow the detection of the onset of diseases at an early stage well before the biochemical abnormalities result in changes in the anatomical structure. Moreover, it will offer efficient methods to monitor the effect of therapeutic treatments. The Molecular Imaging agents provide the crucial link between the specificity of the target and the quantitative visualization of its *in vivo* distribution.

The possibility of carrying out Molecular Imaging protocols by means of MRI is very attractive for the superb anatomical resolution that is attainable by this technique. However, MRI suffers from an intrinsic insensitivity with respect to the competing imaging modalities that has to be overcome by designing suitable amplification procedures based on the development of reporting units endowed with an enhanced sensitivity and on the identification of efficient routes of accumulation of the imaging probes at the sites of interest. MRI definitively suffers when compared to Nuclear Medicine and Optical Imaging techniques for the set-up of Molecular Imaging protocols as its low sensitivity implies the use of 10^7 to 10^9 imaging reporting units per cell [2] when few are necessary for the latter modalities.

In this review, we will survey the MRI nanosized probes and procedures that allow a marked sensitivity enhancement, thus significantly contributing to the development of MR-based Molecular Imaging protocols. First of all, superparamagnetic iron oxide (SPIO, USPIO and MPIO) particles, which have been used in numerous studies aimed at tracking labeled cells and at visualizing targets at low concentration. They have the drawback of generating negative contrast and sometimes it may be difficult to differentiate between signal loss due to the iron oxide particles or native low signal in a given region. Therefore, alternative routes have been designed to produce positive contrast in the vicinity of these particles [3].

We have devoted more attention to the use of paramagnetic Gd(III)-complexes. Along the years, a progressive understanding of the relationships between structure/dynamics and the relaxation process has been fundamental for the development of high sensitive Gd(III) based agents [4].

Now, the need of targeting molecules that are present at very low concentration requires the development of novel classes of contrast agents characterized by an enhanced contrasting ability and improved targeting capabilities. Efficient targeting procedures for cellular labelling and recognition of epitopes characterizing important pathologies are therefore as important as the task of developing nanosized structures containing a huge payload of image contrasting units.

As far as the delivery of a large number of paramagnetic complexes at the targeting sites is concerned, several nanosized systems are currently under intense scrutiny, including dendrimers, micelles (Section 4.1), liposomes (Section 4.2) and other form of lipophilic aggregates as well as natural systems (Section 5) such as apoferritin and lipoproteins.

In general, the high payload of paramagnetic metal ions makes these systems good T_2-susceptibility agents. However, as their use is mainly associated with Gd(III)-complexes with a good water accessibility, they mainly behave as excellent media for the acquisition of T_1-weighted MR images.

Finally, it has been shown that nanosized scaffolds, mostly liposomes, are excellent candidates for the recently proposed class of CEST agents that represent an emerging class of MRI contrast media of huge potential (Section 6). They act as negative agents by reducing the signal intensity of water protons through a saturation transfer mediated by chemical exchange. The great potential of CEST agents lies on the possibility of switching on and off the contrast at will, making possible the detection of more agents in the same region, each uniquely characterized by specific frequency of their mobile protons. Marked sensitivity improvements have been obtained by using as source of mobile protons the water molecules contained in the inner cavity of liposomes, properly shifted by the addition of a shift reagent.

For *in vivo* work, it is particularly important to deal with LIPOCEST agents displaying very large separation between the resonance of the intraliposomal water resonance and the bulk signal. This task has been tackled by generating non-spherical paramagnetic liposomes in which the intraliposomal water resonance receives a substantial magnetic susceptibility contribution.

This survey aims at featuring the recent advances of this field with special emphasis on the systems developed in the authors' laboratory.

2. Iron oxide particles

These materials consist of superparamagnetic iron oxides that are made of ferric (Fe^{3+}) and ferrous (Fe^{2+}) ions [5]. Their peculiar magnetic behavior is associated with the occurrence of domains in their microcrystalline structure that alter markedly the characteristic properties of ferrimagnetism and ferromagnetism such as spontaneous magnetization, residual magnetization, and magnetic hysteresis. These particles (that *per se* are a kind of ferrite and, therefore, ferrimagnetic) are magnetically transformed into a paramagnetic substance. Inside each domain the magnetic moments of the various ions sum up to yield large magnetic moments, in principle analogous to a single paramagnetic ion but of much larger strength, for which they are called superparamagnetic.

Commonly Iron Oxide particles for MRI applications are classified in two classes, namely Superparamagnetic Iron Oxide (SPIO) and Ultrasmall Superparamagnetic Iron Oxide (USPIO) on the basis of the overall size of the protective cover on the surface of the magnetic particle [6]. In fact in both types of particles the iron oxide colloid particles are encapsulated by organic material such as dextran and carboxydextran to improve their compatibility with the biological systems (Fig. 1).

The difference in the overall size of the particles causes marked changes in two important properties as far as concern their use as MRI contrast agents:

(i) upon intravenous administration their blood pool lifetime is strongly affected by their dimensions. USPIO have longer half-life in the blood vessels than SPIO because their smaller size (<50 nm) makes more difficult their uptake from macrophages. On the contrary, SPIO (with diameters of the order of 100–200 nm) are very rapidly removed from the circulation by the reticuloendothelial system (RES). For instance 70–80% of injected AMI-25 particles (size 57–250 nm) are taken up by liver, 6% by the spleen and a small amount by bone marrow [7]. USPIO remains in blood for longer time and more readily accumulate in the lymph nodes and bone marrow;

(ii) in terms of relaxation enhancement properties, the larger magnetic susceptibility of SPIO yields larger R_2/R_1 relaxation rates and higher T_2-shortening effects than those brought about by the smaller USPIO particles.

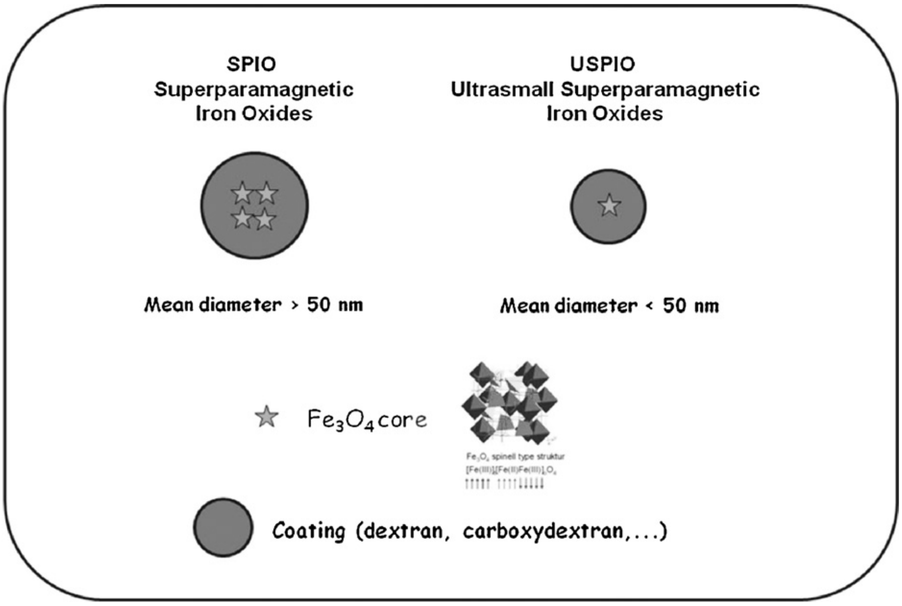

Fig. 1. Schematic view of the composition of Superparamagnetic Iron Oxide particles.

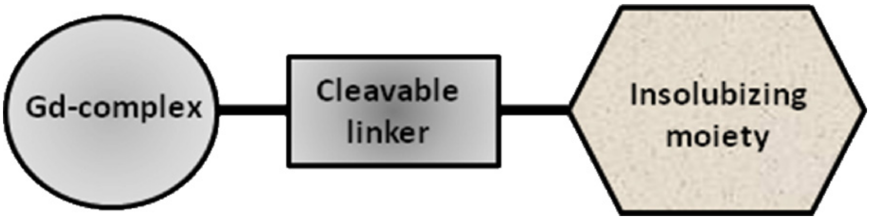

Fig. 2. Schematic representation of an insoluble Gd(III)-based agent designed for switching the T_1 contrast on upon specific cleavage of the linker.

SPIO and USPIO (and also MPIO, the micron-sized iron oxide particles) are under intense scrutiny as tools for cellular labeling for tracking cells' migration, in particular into the nervous system [8]. SPIO work better than USPIO in labeling experiments first of all because the phagocytic uptake increases with the particle size. Cells incubated with SPIOs result in an increase of R_2 upon increasing the local cellular concentration. Typically, R_2 of monocytes labeled with SPIO at the concentration of 1.0 mg Fe/mL is 13.1 s^{-1}. This leads to a detection limit of 58 labeled monocytes per a voxel volume of 0.05 μL [9].

Although SPIO are more suitable for *in vitro* cellular labeling, USPIO are frequently preferred for *in vivo* studies thanks to their

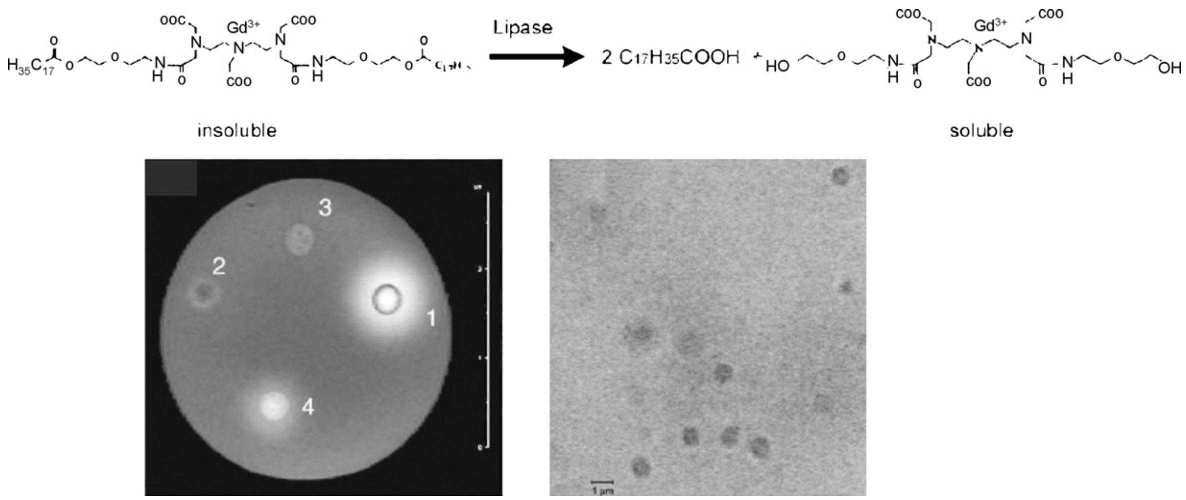

Fig. 3. Top: structure and enzymatic activation of the insoluble Gd(III) complex. Bottom left: the enzymatic activation of the contrast agent is demonstrated on a phantom containing a 1 mM solution of Gd-DTPA as control (1), 2 mM of the insoluble compound (2), a suspension of the enzyme (lipase) (3), and 2 mM of the insoluble compound in the presence of 700 U of lipase. Bottom right: microscopy of the micron-sized particles of the insoluble agent indicates a homogenous size between 0.5 and 1 μm. Adapted from ref. [12].

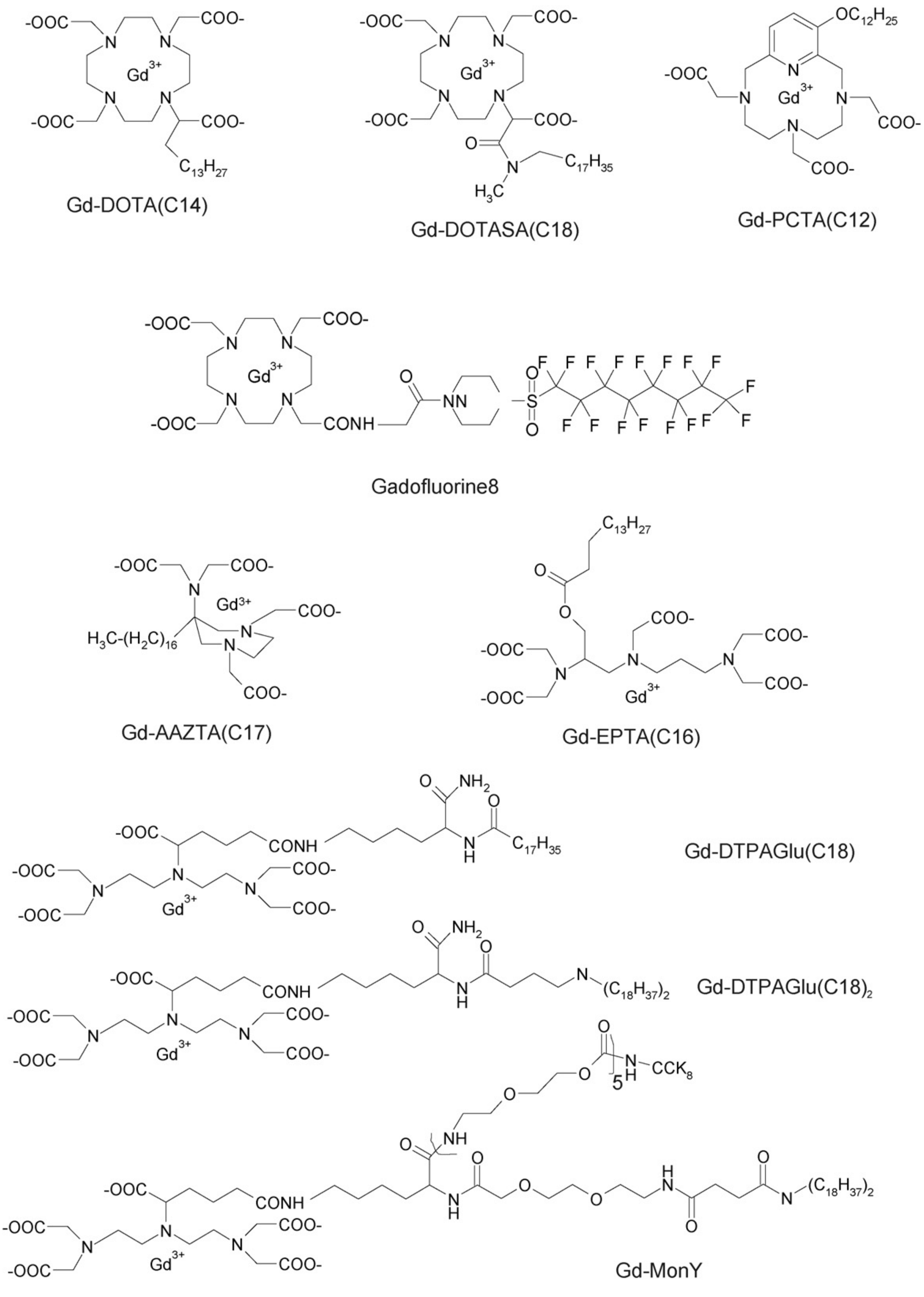

Fig. 4. A collection of Gd(III)-complexes bearing lipophilic moieties that auto-assembly into micelles of interest for MRI applications.

longer blood pool half lifetime. Thus, *in vivo* labeling by USPIO has been pursued in several diseased states, namely stroke [10] and multiple sclerosis [11]. In humans, the lifetime of blood pool is more than 34 h whereas the $t_{1/2}$ of SPIO appears to be shorter than 6 min and such a half lifetime limits their possibility to label endogenous monocytes in circulation.

3. Gd-containing insoluble particles

In analogy to the labeling procedures based on Iron Oxide particles, it is possible to use Gadolinium-loaded particles for labeling cells endowed with phagocytic activity. As particles, they act primary as T_2-susceptibility agents. However, they may trans-

Table 1
Relaxivities (per Gd), water exchange rates, dynamics, micellar size, aggregation number and cmc of paramagnetic micelles of interest for MRI applications

Complex	R_{1p} (mM^{-1} s^{-1})	τ_M (ns)	τ_l (ps)	τ_g (ps)	S^2	r_H	Nagg	cmc (mM)
Gd-DOTA(C14) [14]	22.0 (60 MHz, 25 °C); q = 1	208	820	2220	0.17			0.87
Gd-DOTASA(C18) [14]	17.0 (60 MHz, 25 °C); q = 1	208	330	2810	0.28			0.06
Gadofluorine8 [15]	20.0 (20 MHz, 25 °C); q = 1	*ca.* 1000						<0.001
Gd-EPTA(C16) [16]	22.6 (20 MHz, 25 °C); q = 1	6	330	2100	0.41			0.34
Gd-PCTA(C12) [17]	29.2 (20 MHz, 25 °C); q = 2		τ_R = 473				0.15	
Gd-AAZTA(C17) [18]	30.0 (20 MHz, 25 °C); q = 2	67	295	2540	0.4	5.5 nm	95	0.1
Gd-DTPAGlu(C18) [19]	17.5 (20 MHz, 25 °C); q = 1		τ_R = 650		4.1 nm	60	0.07	
Mixed Gd-DTPAGluC18/CCK8C18 [19]	18.7 (20 MHz, 25 °C); q = 1		τ_R = 700		4.1 nm	58	0.04	
Gd-DTPAGlu(C18)$_2$ [20]	21 (20 MHz, 25 °C); q = 1	81	411	2560	0.45	4 nm		0.096
MixedGd-DTPAGlu(C18)$_2$/CCK8(C18)$_2$ [20]	18.6 (20 MHz, 25 °C); q = 1	81	406	2190	0.43			0.044
Gd-MonY [21]	15.03 (20 MHz, 25 °C); q = 1	60	255	2800	0.35	4.8 nm	34	0.0015

form upon time into T_1-agents provided that they are properly designed in order to be responsive to the activity of a specific enzyme.

The general scheme for such agents is reported in Fig. 2.

The insolubilizing moiety promotes the formation of particles that dissolve upon the action of the enzyme capable of cleaving the linker. This process generates soluble Gd(III)-complexes that act as T_1-agents and the increase of the longitudinal relaxation rates of their solutions is therefore reporting on the activity of the cleaving enzyme.

The first proposed example [2] was a system containing an esterase function between the Gd chelate and the insolubilizing moiety represented by a long aliphatic chain (Fig. 3).

Upon formation of the Gd(III) complex in water, the system forms a precipitate that can be drilled to yield particles of diameter close to 1 μm. The particles, when put in contact with a hydrolitic enzyme, progressively solubilize to yield an aqueous solution of the Gd complex.

From the measure of the relaxation rate of the water solvent protons one may obtain an estimate of the amount of the Gd(III) complex that passed in solution and, in turn, on the extent of the specific enzymatic activity.

The method has been applied to label different cell types characterized by phagocytic activity. In particular astrocytes labeled in this way [12] have been introduced in rat brain and tracked up to a couple of weeks after the inoculation (Fig. 3). Much work is cur-

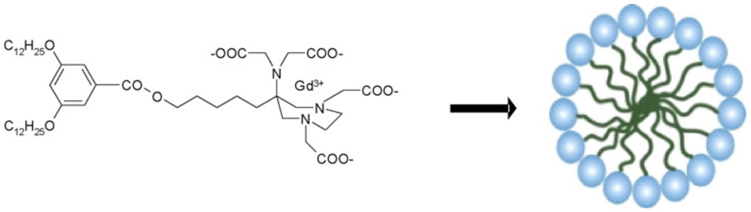

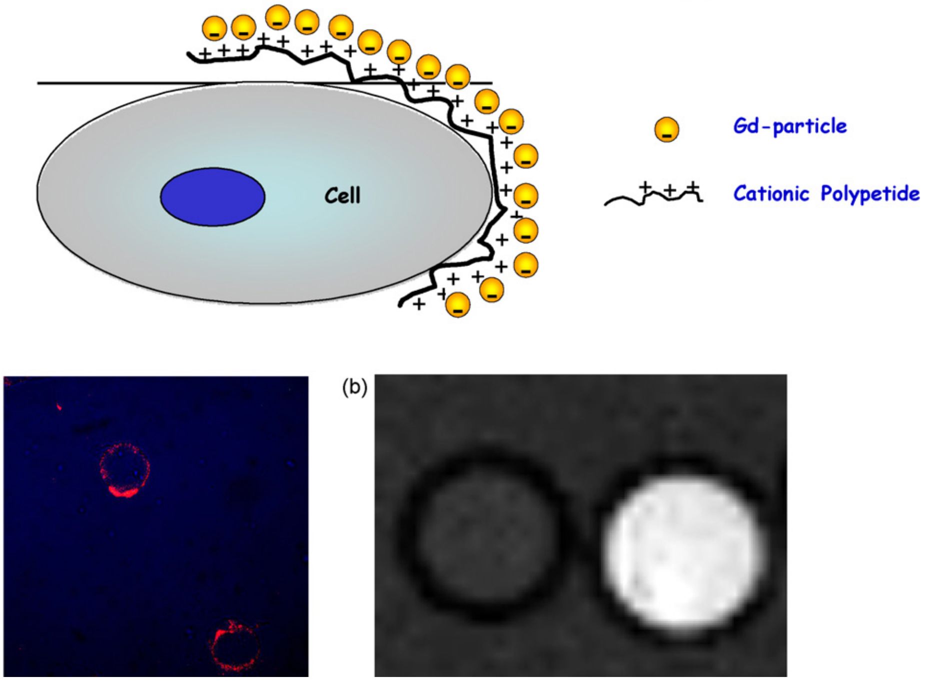

Fig. 5. The design of the high sensitivity MR-imaging reporter. (a) The binding of the supramolecular adduct at the cell membrane through the intermediation of the cationic linker is validated by the confocal microscopy images obtained by using a Gd-containing nanoparticle doped with a rhodamine-phospholipid and polyarginine. (b) MRI of cellular pellets in agar. The cells labeled with polyarginine/Gd-nanoparticles (right) contains approximately 6×10^9 Gd per cell and display a T_1 value of 334 ms to be compared witha T_1 of 2064 ms of the unlabeled cells (left). Adapted from ref. [24].

rently done to assess the potential of this method to report about the activity of proteases that are enzymes of outstanding importance in several patho-physiological processes that involve tissue remodeling.

4. Auto-assembled systems containing paramagnetic complexes

4.1. Micelles

Paramagnetic micelles have often been considered as contrast agents for MRI applications [13]. To this end, several Gd-complexes bearing lipophilic substituents have been reported (Fig. 4 and Table 1).

These molecules form aggregates in which the hydrophobic portions are oriented within the cluster and the hydrophilic moieties (containing the Gd-probe) are exposed to the solvent. Depending on the length and the number of the hydrophobic chains and on the nature of the hydrophilic heads, the obtained micelles are characterized by different size and shape (spherical, cylindrical, vesicular).

The observed relaxivities (expressed as $(\mathrm{mM_{Gd}\,s})^{-1}$) are basically determined by the number (q) of water molecules in the inner coordination sphere of the paramagnetic metal ion. In fact, almost all the $q = 1$ systems have relaxivity values in the range 18–23 $(\mathrm{mM_{Gd}\,s})^{-1}$ and the $q = 2$ systems 29–30 $(\mathrm{mM_{Gd}\,s})^{-1}$. Only one system (MonY) [21] is endowed with a relaxivity value that is slightly lower than the others, likely because of the structural differences of the monomeric complex. In fact, this system is Y-shaped and contains the three moieties required for a micellar targeting system: (a) the hydrophobic chains that allow the micellar aggregation, (b) the Gd-complex and (c) a bioactive peptide (CCK8) for target recognition. Moreover, as indicated by DLS (Dynamic Light Scattering) and SANS (Small Angle Neutron Scattering) measurements, this system aggregates in aqueous solution to give ellipsoidal micelles rather than the spherical conventional ones.

Basically, the relatively low relaxivity values shown by the paramagnetic micelles depend on the non-optimal dynamic regime of these systems, which is characterized by the occurrence of a fast local motion of the Gd-containing cage at the surface of the micelle overlapped to a slower global motion of the supramolecular aggregate.

An accurate determination of the parameters governing the reorientational dynamic may be pursued through the quantitative analysis of the NMRD (Nuclear Magnetic Relaxation Dispersion) profiles, which report the relaxivity as a function of the applied magnetic field strength. The analysis of the NMRD profiles of micelles containing solutions is frequently performed by using the Solomon–Bloembergen–Morgan equations modified according to the model-free approach developed by Lipari and Szabo for non-extreme narrowing conditions [22,23]. By this approach, it is possible to distinguish between a local faster motion (governed by τ_l) and a global slower motion (governed by τ_g). The extent of the local and global contributions to the overall motion is measured by an order parameter (S^2) that can range between 0 and 1. The analysis of the NMRD profiles according to this model for the systems reported in Table 1 gave very similar τ_l, τ_g and S^2 values on top of similar relaxivities and structural features.

On this basis, the limiting factor to the attainment of higher relaxivities seems to be the rotational dynamic; in fact, the relaxivity appears invariantly lower than the expected value because the internal motions are faster than the overall tumbling of the micellar system.

Furthermore, Merbach and co-workers demonstrated that the dipolar interactions between nearby paramagnetic centres in micellar systems increase the transverse electronic relaxation of the electron spins of Gd(III) which, in turn, reduces the attainable relaxivity [15]. This drawback may be removed by diluting the Gd(III) ions with diamagnetic Y(III) ions in order to increase the average distance between neighbouring Gd(III) ions. This approach has also been exploited by Aime and co-workers, who reported a relaxivity enhancement of *ca.* 40%, over all the investigated frequency range (between 0.01 and 80 MHz), for AAZTA(C17) mixed micelles formed by 2% of Gd(III) and 98% of Y(III) ions [18].

4.1.1. Targeted micelles

Thanks to their dimensions, micelles act as long circulating blood pool agents. They may also actively bind to serum components as it has been recently reported for Gd-AAZTA(C17), whose micelles associate very strongly to HSA ($K_A = 1.5–1.7 \times 10^5\ \mathrm{M}^{-1}$) owing to the electrostatic interactions among the negative charges of the micelles and the positively charged residues on the surface of the protein [18].

This observation prompted an innovative application of electrically charged micelles in cellular labeling procedures [24].

The aim of this work is to anchor, on the cell-surface, particles containing a high number of paramagnetic Gd(III)-complexes without compromising the overall characteristics of the cell membrane. The paramagnetic particles consist of self-assembled lipophilic Gd-AAZTA$(\mathrm{C16})_2$ complexes (Fig. 5).

The presence of two long aliphatic chains and the aromatic moiety endow this amphiphilic complex with a very high tendency to aggregate in aqueous media. Already at monomer concentration as low as 1×10^{-5} M the system appears to be present in an aggregated form (likely discoidal aggregates) characterized by a relaxivity of 25 $(\mathrm{mM_{Gd}\,s})^{-1}$ at 298 K and 20 MHz, a diameter of *ca.* 80 nm (with a very low polydispersity index) and an aggregation number of *ca.* 850. The anchoring of the paramagnetic particle on the cell surface has been performed exploiting a cationic linker (Polyarginine) that binds to the negative charges either on the particles and the membrane surface. By using 1.1×10^8 Polyarginine molecules per cell, it has been found that each cell can load up to *ca.* 5×10^6 particles. This corresponds to *ca.* 5×10^9 Gd/cell, i.e. well above the threshold for MRI visualization.

Paramagnetic micelles may also be used for targeting specific sites through the conjugation of proper vectors to their surface. Recently, Accardo et al. reported the synthesis and the characterization of different kinds of tumor-specific mixed micelles containing a bioactive peptide (CCK8) specific for cholecystokinine receptors (over-expressed in many tumors) and Gd-containing moieties, both functionalized with one [19] or two [20] long hydrophobic chains to promote the micellization step. All of these mixed micellar supramolecular aggregates, even if not yet tested *in vivo*, appear to be promising candidates as tumor-specific MRI contrast agents.

Raatschen et al. described the MRI tumor-characterizing potential of a new protein avid contrast agent, GadofluorineM, which enhances the tumor signal according to the malignancy of the lesion [25]. The reported results show a potential utility for differentiating benign and low-grade malignant lesions from high-grade cancers.

Gadolinium-containing immune-micelles (diameter: 89 nm, relaxivity (at 298 K and 60 MHz) of 25.7 $(\mathrm{mM_{Gd}\,s})^{-1}$) have been used to detect atherosclerosis either *in vitro* [26] or *in vivo* [27] by targeting the Macrophage Scavenger Receptors (MSR). In fact, MSR, a macrophage specific cell-surface protein, is significantly over-expressed on atherosclerotic macrophages and foam cells, while it is not expressed on normal vessel wall cells. *In vivo* MRI experiments (Fig. 6) revealed that 24 h post-injection immune-micelles yielded a 79% increase in signal intensity of the atherosclerotic aortas in ApoE−/− mice compared with only 34% using untargeted micelles, whereas no enhancement was detected using Gd-

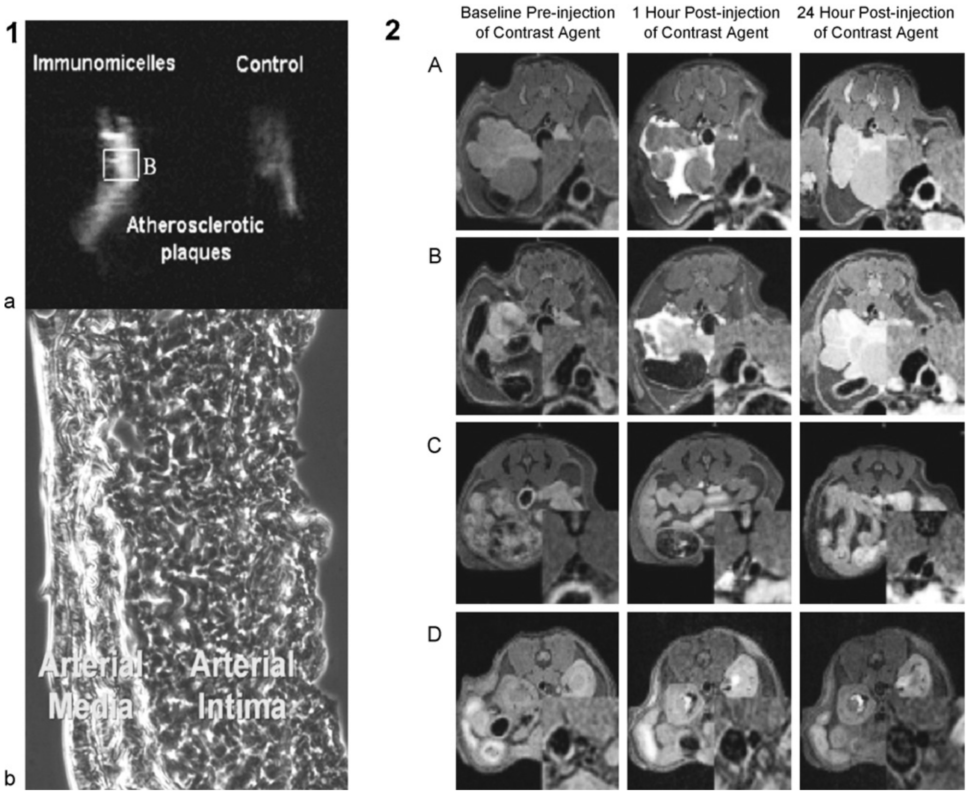

Fig. 6. *Ex vivo* MR images comparing a longitudinal section through the arterial wall of an ApoE KO Aorta incubated with immune-micelle and with DMEM control; (1b) Black and white image of the above aorta using green fluorescence confocal microscopy, demonstrating the degree of plaque burden. (2) *In vivo* MRI images at baseline and post-injection of immune-micelles (A and B), untargeted micelles (C) and Gd-DTPA (D) in ApoE−/− mice. Adapted from ref. [27].

DTPA. Confocal laser-scanning microscopy revealed co-localization between fluorescent immune-micelles and macrophages in plaque.

Atherosclerotic plaques have been recently detected also with GadofluorineM-enhanced MRI [28]. The significant uptake of the micellar contrast agent into atherosclerotic plaques, combined with its high relaxivity, led to an increased signal intensity of plaques on T_1-weighted images (Fig. 7). Although the exact mechanism of GadofluorineM uptake is not completely understood, the authors hypothesized that this micellar contrast agent endowed with a long plasma half-life would accumulate in atherosclerotic plaques because of enhanced endothelial permeability and increased interstitial space.

4.2. Liposomes

Liposomes are nanosized vesicles in which an aqueous core is encapsulated by one (unilamellar) or more (multilamellar) phospholipidic bilayers. A further sub-classification divides the unilamellar vesicles (UV) in small (SUV, diameter of 50–150 nm) and large (LUV, 150–800) liposomes according to their size. As soon as they were discovered [29], it was immediately recognized the great relevance that such systems could have in the biomedical field as model systems for studying biological membranes and as drug carriers. As far as concern the latter application, the main strong points in favour of liposomes are: (i) high biocompatibility, (ii) easiness of preparation, (iii) possibility to carry hydrophilic, amphiphilic and lipophilic molecules, (iv) possibility of modulating the pharmacokinetic properties by changing the chemical composition of the bilayer. All these properties make liposomes excellent nanocarriers for MRI applications, because, in addition to act as carriers of contrast agents, their peculiar properties can be successfully used for improving the contrastographic efficiency of the trans-

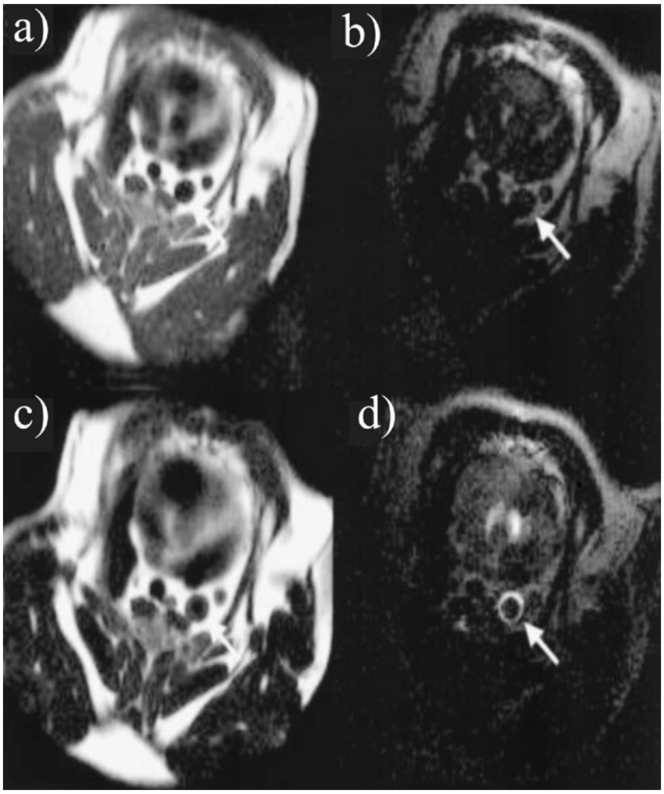

Fig. 7. HASTE (a and c) and IR TurboFlash (b and d) images before (a and b) and 48 h after (c and d) application of GadofluorineM in 18-month-old WHHL rabbit at identical slice position. Adapted from ref. [28].

ported agent, as well as for generating new contrast mechanisms (see Sections 4.2.2 and 6).

4.2.1. Paramagnetic liposomes as T_1-agents

The first reports about the use of liposomes loaded with T_1-shortening MRI agents were published in the late 1980s and dealt with the encapsulation of high amounts (hundreds of millimolar) of hydrophilic paramagnetic ions as Mn(II) [30] or Mn(II)- and Gd(III)-complexes [31–34] in the aqueous core of the vesicle.

The resulting paramagnetic vesicles were mainly used as carriers for the deliver of the imaging agents to pathological tissues, mostly tumors, where the liposomes are expected to passively accumulate thanks to the Enhanced Permeability and Retention (EPR) mechanism [35,36]. This process allows the accumulation of nanosized systems in regions of neo-angiogenesis characterized by a high vascular permeability accompanied with an inefficient lymphatic drainage.

The successful MRI visualization of several tumors on animal models (including the detection of liver metastasis) after the i.v. injection of T_1-shortening liposomes is primarily the result of the high relaxivity of the nanosized vesicles that carries hundreds of thousands of imaging reporters. However, it is worth noting that the relaxation enhancing efficacy of a single imaging reporter is considerably "quenched" when it is encapsulated in the liposome. As an illustrative example, the millimolar relaxivity of the clinically approved Gd-HPDO3A complex decreases of about one order of magnitude on going from 3.75 $(\text{mM}_{\text{Gd}}\,\text{s})^{-1}$ for the non-encapsulated compound to 0.3 $(\text{mM}_{\text{Gd}}\,\text{s})^{-1}$ (values measured at 0.47 T and 310 K) when the imaging reporter is entrapped in the liposome cavity [34]. It has been demonstrated that this "quenching" effect is inversely proportional to the water permeability of the liposome bilayer and to the size of the vesicle, and it is directly dependent on the concentration of the paramagnetic system inside the vesicle.

The relaxivity "quenching" caused by the encapsulation of the imaging reporter has been exploited for designing responsive agents in which the water permeability of the bilayer or the overall integrity of the vesicles is made sensitive to physicochemical variables of theragnostic relevance. Two representative examples can be found in the classes of pH and temperature responsive agents. In the former case, the imaging reporter is encapsulated in liposomes whose bilayer contains components that change their structure (and charge) as a function of pH. A typical combination of amphiphiles that confer to the bilayer a pH-responsiveness tuned at the physio-pathological values is represented by phosphatidylethanolamine (PE)-based phospholipids and dipalmitoylglycerosuccinate (DPGS). Lokling et al. [37] demonstrated that the pH relaxometric profile in human blood of liposomes encapsulating Gd-DTPA-BMA can be modulated according to both the length of the diacyl chains of the PE component and the amount of the DPGS component incorporated in the bilayer (Fig. 8) [37].

Importantly, these liposomes showed a limited leakage of the imaging reporter in blood at physiological pH. It was suggested that the relaxivity enhancement displayed by these systems at low pH values results from the leakage of the imaging reporter caused by the vesicle aggregation induced by the change of their surface charge. To support this view, the same research team reported that the encapsulation of a Gd(III) complex endowed with a high affinity to serum albumin significantly improved the relaxometric response at low pH in blood thanks to the well-known relaxation enhancement occurring when the complex, released from the liposomes, binds the serum protein [38].

As far as the temperature reporters is concerned, liposomal MRI probes able to switch on the T_1 contrast in a narrow temperature range has been designed by selecting phospholipidic components with a well-defined gel-to-liquid crystalline transition phase temperature (T_m), like distearylphosphatidylcholine (DSPC, T_m of about 329 K) or dipalmitoylphosphatidylcholine (DPPC, T_m of about 314 K) [39]. At temperature higher than T_m the liposome bilayer increases its fluidity and the water diffusivity. In addition, also the stability of the vesicle decreases and the consequent release of the encapsulated imaging reporter accounts for the observed relaxivity enhancement. Fig. 9 reports the comparison between the temperature dependence of the relaxivity of Gd-DTPA-BMA free and encapsulated in DSPC-based liposomes [33].

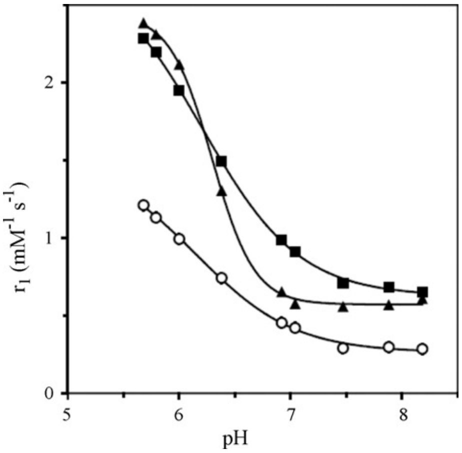

Fig. 8. r_1 relaxometric pH dependence of dipalmitoylPE/DPGS liposomes encapsulating Gd-DTPA-BMA containing 10 mol% (filled squares) and 30 mol% (upper triangles) of DPSG, and distearylPE/DPGS containing 10 mol% of DPGS (open circles) after 20 min of incubation in buffered human whole blood (0.47 T, 310 K). Adapted from ref. [37].

The data highlights the relaxivity "quenching" occurring at temperature values lower than T_m caused by the low water permeability of the DSPC bilayer, and its release when the temperature is approaching the phase transition temperature.

This temperature-sensitive liposomal MRI agent has been also successfully tested *in vivo* with the aim of guiding hypertermia ablation in a tumour model on rabbit liver [40].

Fig. 10 reports a series of T_{1w} MR images obtained during the localized RF heating of the tumour (indicated by a white arrow), which clearly indicate the appearance of a bright region in the surrounding of the treated lesion caused by the release of the Gd(III) chelate from the temperature-sensitive liposomal agent.

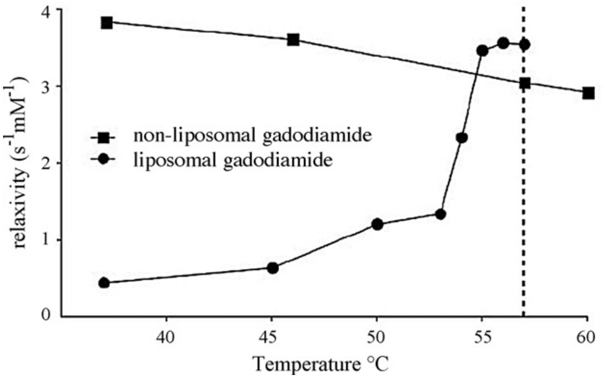

Fig. 9. Temperature dependence of the relaxivity for Gd-DTPA-BMA free (squares) and encapsulated in DSPC-based liposomes (circles). The vertical dashed line indicates the T_m value of the bilayer. Adapted from ref. [40].

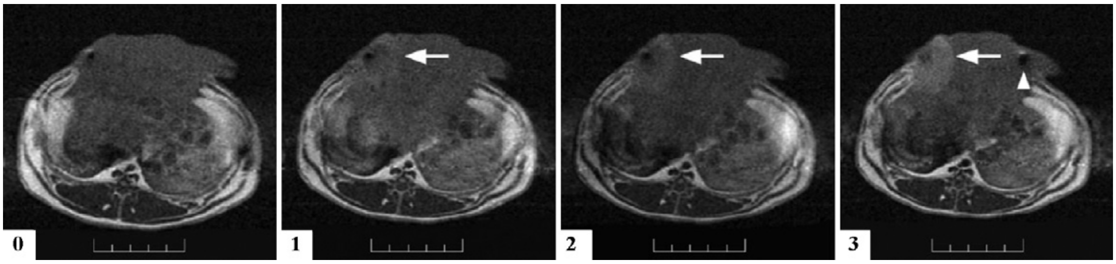

Fig. 10. T_{1w} MR images of RF ablation in rabbit liver after i.v. injection of the liposomal contrast agent at different steps: prior heating (t0), during heating (t1), after normalization of tissue temperature (t2), and 15–20 min after normalization of tissue temperature (t3). Note the increasing of the signal intensity in the periphery of the lesion (white arrow). Adapted from ref. [40].

A more exhaustive list of examples illustrating the great potential of the so-called thermosensitive liposomes (TSL) for guiding heating-based therapies is reported in the review by Lindner et al. [41].

An improvement of the potential of TSL has been recently reported by Terreno et al., who proposed a method, based on the measurement of the ratio between the paramagnetic contributions to the transverse (R_{2p}) and the longitudinal (R_{1p}) relaxation rates, which allows the use of the MRI response independently of the knowledge of the actual concentration of TSL [42].

Other important applications of TSL are in the field of drug delivery imaging. A first example was published by Viglianti et al. [43], who prepared a sterically protected TSL based on DPPC and containing 10 mol% of a lysolipid (MSPC) that is known to facilitate the drug release from the vesicle. The antitumoral drug Doxorubicin was actively loaded in the liposome cavity already containing $MnSO_4$ as T_1 agent. Upon heating at temperature higher than its T_m (>313 K) the relaxivity of the system increases owing to the release of Mn(II) ions which, in turn, reports about the drug delivery process. This system was also tested *in vivo* on rats bearing a xenografted fibrosarcoma. The T_{1w} MR images showed a rapid and sustained bright contrast at the periphery of the lesion exposed to the heating.

In principle, the improvement of the T_1-relaxing efficiency of liposomes encapsulating the imaging reporter can be pursued by utilizing small sized vesicles (SUV) endowed with high water permeable bilayer, but, unfortunately, the increase of the water diffusivity of the membrane is usually accompanied with a significant decrease of the *in vivo* stability of the liposome. An alternative approach consists of designing liposomes in which the imaging reporter is incorporated in the vesicle bilayer.

The relaxivity enhancement of the incorporated imaging reporter with respect to the encapsulated one relies on the lengthening of the reorientational correlation time, τ_R, of the former system, that improve the efficiency of the dipolar coupling between the unpaired electrons of the paramagnetic ion and the water protons. Since this coupling is function of the magnetic field strength, the NMRD profiles of liposomes incorporating Gd(III)-complexes are characterized by the typical relaxivity hump, centred at about 1 T, usually observed for slow-tumbling paramagnetic systems [44,45]. The relaxation enhancement of liposomes incorporating Gd(III)-complexes is determined by the structural and dynamic properties of the coordination cage of the metal complex. The most relevant parameter is the water exchange rate, k_{ex}, of the metal coordinated water that has to be finely tuned in order to maximize the overall relaxivity of the system. It has been calculated that k_{ex} values of 10^8 to 10^9 s^{-1} are optimal for achieving highest relaxivities [46]. Two routes have been followed for conjugating the lipophilic chains to the coordination cage of the metal complex: (i) through the formation of amide bonds involving the carboxylic groups of the acyclic ligand DTPA, and (ii) through linkages that minimize the chemical characteristics of the donor atoms of macrocyclic (DOTA-based) ligands. The first approach has been extensively used, mainly for the relative easiness in the ligand synthesis, but it has two major disadvantages: (i) the thermodynamic and kinetic stabilities of DTPA amides appear too low for the set-up of safe *in vivo* applications as those required in typical Molecular Imaging protocols [47], and (ii) the k_{ex} values for this type of coordination cage is much lower than optimal ($\leq 10^6$ s^{-1}), thus “quenching” the relaxivity attainable with these nanoprobes. Conversely, DOTA-like macrocyclic structures, besides a much higher chemical stability, display k_{ex} values closer to the optimum, even if one of the carboxylate groups is functionalized with the lipophilic tail/s through an amidic bond. Support to this view is nicely gained by comparing the relaxivities measured at 0.47 T for the membrane incorporated Gd(III)-complexes of bis-stearylamide DTPA (ranging from 8 to 12 $(mM_{Gd}\ s)^{-1}$ depending on temperature and liposome formulation) [48,49] and for the corresponding systems incorporating the amphiphilic DOTA-based compounds (from 25 to 45 $(mM_{Gd}\ s)^{-1}$) [45,50].

Liposomes incorporating Gd(III)-complexes have been successfully used in many *in vivo* MRI applications on animal models

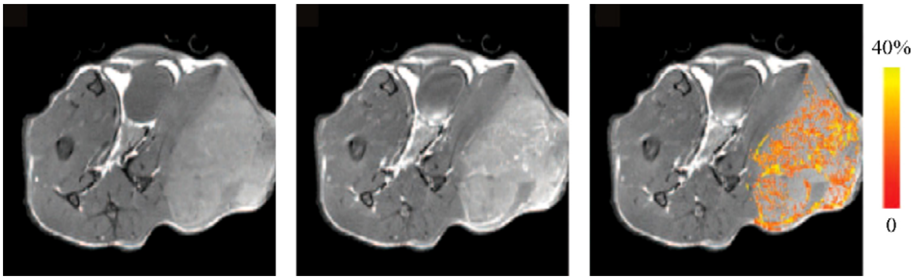

Fig. 11. MR images on a xenografted tumor animal model before (left image) and after (middle image) injection with paramagnetic liposomes targeting a neo-angiogenesis marker ($\alpha_v\beta_3$ integrin) and incorporating a Gd(III)-complexes. Pixels in tumor with signal enhancement of at least 5 times the noise level were color coded (right image). Adapted from ref. [52].

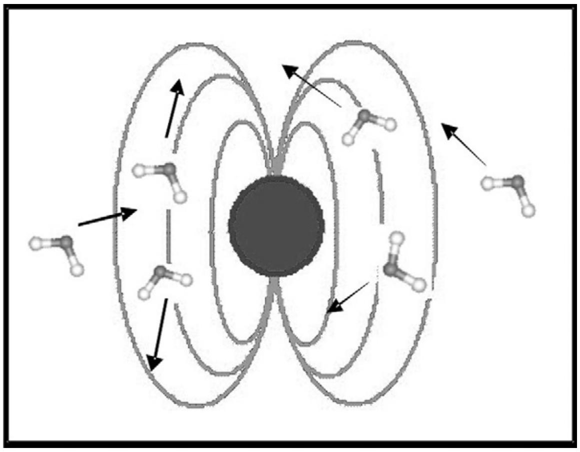

Fig. 12. Schematic view of the interactions between the magnetic field gradients created by a paramagnetic nanoparticle and water molecules diffusing around it.

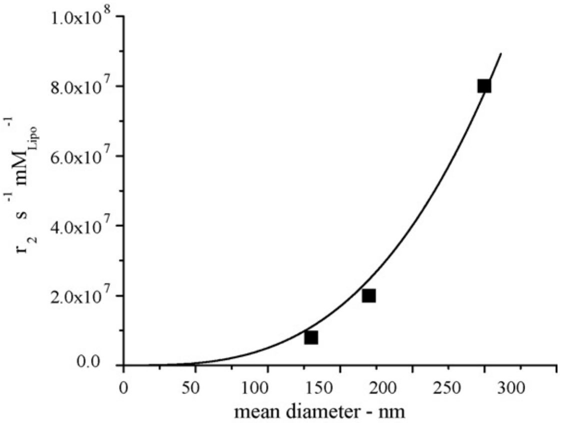

Fig. 14. Size dependence of the transverse relaxivity (normalized to the liposome concentration) of POPC/Chol/DSPE-PEG2000 (55/40/5 in moles) liposomes encapsulated with a 200 mM solution of Gd-HPDO3A (14 T, 298 K). The line was only drawn for guiding eyes.

including the visualization of tumors either by passive [48] or active [51,52] targeting (Fig. 11), detection of atherosclerotic plaques [53], lymph nodes [54], inflammation sites [55], and visualization of myocardium infarcted areas [56].

Interestingly, the selective tumor distribution of paramagnetic liposomes targeting an angiogenesis marker ($\alpha_v\beta_3$ integrin) has been recently exploited for *in vivo* monitoring the therapeutic efficacy of antiangiogenetic drugs by MRI [57].

An additional advantage of using nanosized assembled systems deals with the novel frontier of multimodal imaging. Liposomes appear excellent systems for designing probes containing imaging reporters that can be visualized with different imaging modalities. Most of the work in this field has been carried out by combining MRI and Optical imaging probes and it has been recently reviewed by Mulder et al. [58].

4.2.2. Paramagnetic liposomes as T_2-susceptibility agents

In the late 1980s, it was reported that paramagnetic low molecular weight Dy(III)-complexes can act as T_2-susceptibility agents in MRI images when they are unequally distributed in vessels and in the surrounding tissues [59,60]. The effect can be further enhanced when the paramagnetic complexes are entrapped in vesicles such as liposomes [34,61]. The observed behavior is well accounted for in terms of the field gradients created by the compartment containing the paramagnetic ions that induce the spin dephasing of the water protons diffusing in the outer region of the compartment Fig. 12.

It is straightforward to note that any nanosized system containing paramagnetic metal ions would act as a T_2-susceptibility agent. In this context, paramagnetic liposomes have a high potential owing to the high payload of paramagnetic complexes that can be either entrapped in their inner cavities or, upon suitable functionalization with lipophilic substituent, be incorporated in their membrane bilayer [62].

Fig. 13 (on the left) compares the R_2 values measured for an aqueous suspension of paramagnetic liposomes encapsulating DyHPDO3A and an aqueous solution containing the same total concentration of the paramagnetic metal ion. The transverse relaxation rate of the nanosized system is almost one order of magnitude higher at the magnetic field strength of 7 T. The R_2-enhancement generated by the susceptibility effect is also evident in the *in vitro* MR image (Fig. 13 on the right).

When normalized to the liposome concentration (in mmol/L), the transverse relaxivity ranges from 10^6 to 10^9 $(\mathrm{mM_{Lipo}\,s})^{-1}$ (depending on the size and on the amount of paramagnetic complex) at 7 T and 298 K. The high T_2-relaxing efficiency displayed by these nanoprobes makes them very suitable for Molecular Imaging purposes.

The T_2-susceptibility effect is also markedly dependent on the size of the vesicle entrapping the paramagnetic species as reported in Fig. 14, where the transverse relaxivities of liposomes with different size, but filled up with the same concentration of Gd-HPDO3A, are compared. The reported R_2-enhancement results from the increase of the number of paramagnetic centres encapsulated in the liposome cavity, which is proportional to vesicle volume.

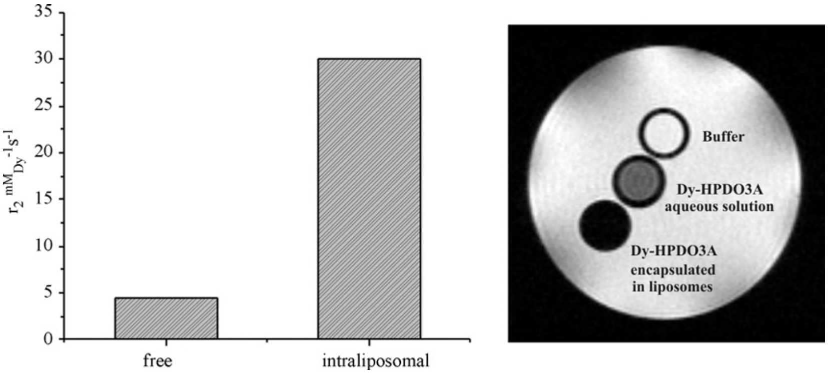

Fig. 13. Left: Effect of the liposome compartmentalization of a paramagnetic complex (Dy-HPDO3A) on the transverse rates at 7 T and 312 K. Right: *In vitro* RARE T_{2w} MR image obtained at 7 T and 312 K.

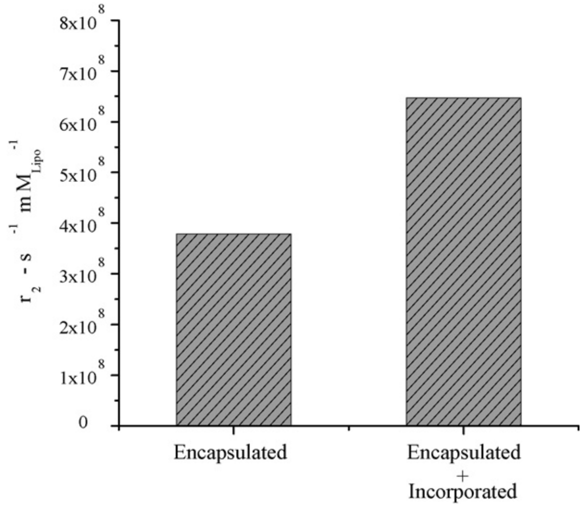

Fig. 15. Transverse relaxivity (normalized to the liposome concentration) of Dy-loaded liposomes (mean hydrodynamic diameter 130 nm) in which the paramagnetic centers are encapsulated (Dy-HPDO3A) or encapsulated (Dy-HPDO3A) and incorporated (amphiphilic Dy(III) complex, 20 mol%) in the liposome bilayer made of DPPC/DSPE-PEG2000 (7 T, 312 K).

The most efficient T_2-susceptibility agents are represented by liposomes that contain the paramagnetic labels either encapsulated in their inner cavity or incorporated in their membrane bilayer (Fig. 15).

As the susceptibility effect increases with the applied magnetic field strength, T_2-liposomes work well at high fields. Fig. 16 reports the field-dependent T_2 contrasting ability of a typical Dy-HPDO3A encapsulating liposome.

Finally, it is expected that susceptibility effects are also dependent on the magnetic moment of the paramagnetic ion entrapped in the vesicle cavity. Fig. 17 shows a comparison among the transverse relaxation rates of liposomes of similar size loaded with different Ln-HPDO3A complexes (Ln = Dy, Gd, and Tm). The left side of the figure displays the qualitative correlation between the R_2 values (normalized to the millimolar Ln concentration) and the effective magnetic moment (μ_{eff}) of the encapsulated metal ion.

Quantitatively, it is important to note that the ratio between the r_2 values fairly corresponds to the square of the ratio of the corresponding μ_{eff} values, thus confirming that Dy(III) loaded liposomes are the most efficient systems in this class of agents.

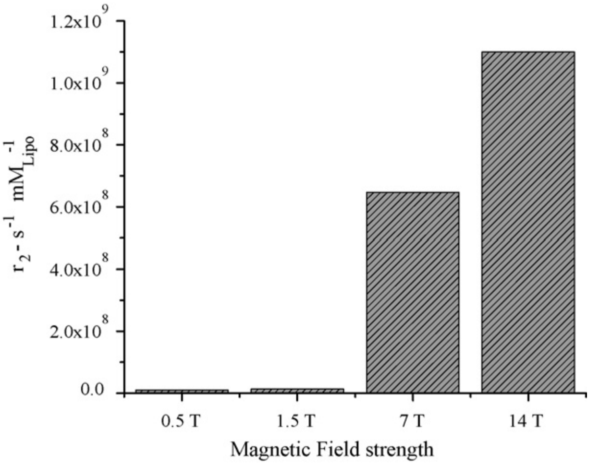

Fig. 16. Magnetic field dependence of the transverse relaxivity (normalized to the liposome concentration) of liposomes (mean hydrodynamic diameter 220 nm) encapsulating Dy-HPDO3A (312 K, liposome membrane DPPC/DSPE-PEG2000 95/5 mol%).

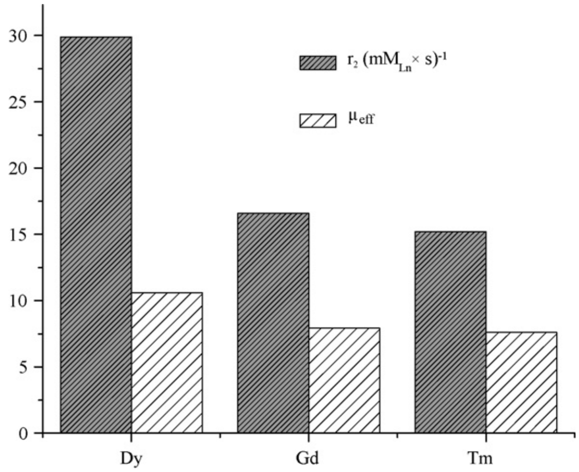

Fig. 17. Histogram reporting the correlation between the transverse relaxation rate (normalized to the millimolar concentration of the Ln ion, 7 T, 298 K) of liposomes encapsulating Ln-HPDO3A complexes and the effective magnetic moment of the Ln(III) ions (liposome formulation POPC/Chol/DSPE-PEG2000, 55/40/5 mol%, mean diameter 170 nm).

Another class of liposome-based T_2-susceptibility agents are represented by magnetoliposomes, in which iron oxide particles (acting as T_2 MR agents as already described in Section 2) are encapsulated in liposomes [63]. Such systems are of interest in therapy owing to their interaction with externally applied magnetic fields, which allows them to be used in magnetic targeting experiments [64], as drug delivery carriers [65], or in hyperthermia treatments [66].

As far as their applications in MR-Molecular Imaging is concerned, magnetoliposomes have been successfully used as blood pool agents [67], for targeting bone marrow [68], and solid tumors [69].

5. Naturally occurring nanosized systems

This section deals with naturally occurring nanosized carriers that may be loaded with paramagnetic metal complexes in order to yield MR-imaging probes. As the level of modification introduced by the loading of the paramagnetic complexes is minimal, the major advantages associated with these probes are: (i) absence of immunological reactions; (ii) limited uptake by macrophages and (iii) maintenance of targeting and biodistribution properties of the parent species.

5.1. Gd-loaded apoferritin

The first reported system is represented by Gd-loaded apoferritin [70]. Ferritin is the protein devoted to the storage of iron in cells. It may host up to 4500 iron atoms organized as oxy–hydroxy polymeric chain. Ferritin consists of 24 proteins that self-assemble by means of saline and hydrogen bonds to yield a spherical aggregate containing the iron core. The supramolecular proteic adduct displays 10 channels for communicating between the inner and outer compartments in order to provide a pathway for the recruitment of iron ions. It was known from several years [71] that it is possible to replace *in vitro* the iron core in the inner cavity of ferritin with other materials, for instance drugs or prodrugs, to yield drug delivery carriers or to use the inner cavity as a reactor to produce magnetic particles. The method to entrap exogeneous molecules in

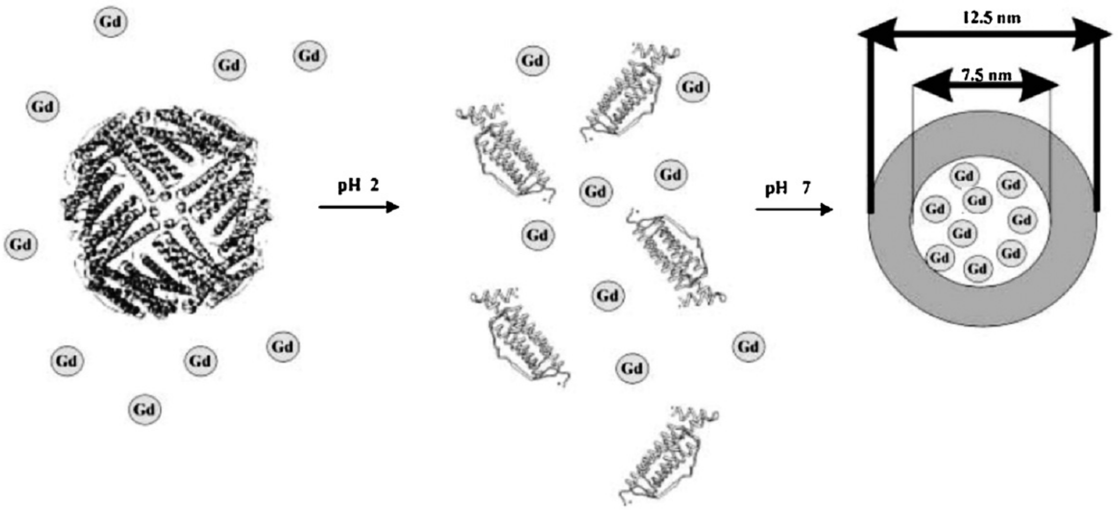

Fig. 18. Schematic view of the strategy for entrapping Gd(III)-complexes in the apoferritin cavity. Adapted from ref. [70].

the apoferritin cavity consists of:

(i) disassembling the supramolecular aggregate by lowering the pH of the solution to 2. In this way the protonation of aminoacid residues modifies the charge distribution with the net result of the collapse of the supramolecular aggregate with the release of its components;

(ii) re-assembling of the apoferritin cage by changing the pH from acid to neutral. By carrying out this operation in the presence of the species that one wants to entrap, the resulting apoferritin will be properly loaded.

The re-constructed apoferritin loaded with the desired molecules has to be dialyzed in order to remove the non-entrapped materials as well as it has to be purified (by HPLC) in order to separate non-assembled or wrongly assembled protein chains.

The overall process is summarized in Fig. 18.

The best MRI agents for the entrapment process are represented by neutral complexes like Gd-DTPA-BMA and Gd-HPDO3A, the latter is preferred because of its higher stability at acidic pH values. We found that it is possible to entrap up to 8–10 Gd-HPDO3A molecules per apoferritin. The entrapped molecules are too large to enter the channels and then remain sequestered in the inner cavity of the protein aggregate. Conversely, water molecules can freely get in and out the cavity thus allowing the paramagnetism of the MRI contrast agent to be transferred to the “bulk” water molecules. Very interestingly the relaxivity of Gd-HPDO3A entrapped in the apoferritin cavity shows a relaxivity that, at 20 MHz, is *ca.* 20 times higher than that of the free Gd-HPDO3A complex. From the characteristics of the NMRD profile (Fig. 19) it is evident that an important role is played by the elongation of the molecular reorientational time but other peculiar contributions are also present. For instance, the characteristics of the aminoacid residues facing the inner ferritin cavity appear to provide an additional source of exchangeable protons that act as a kind of extended “second coordination sphere” for Gd-HPDO3A molecules interacting with the charged moieties at the inner protein surface.

This was later proved by Sherry and co-workers by entrapping a Gd complex which does not contain any water molecule directly coordinated to the paramagnetic metal ion [72]. Nevertheless, such a complex when entrapped in the apoferritin reaches the relaxivity of *ca.* 60 $\mathrm{mM^{-1}\,s^{-1}}$. Still is debated the potential contribution associated to multiple interactions that the water molecules may have with the paramagnetic complex before getting out of the protein cavity.

As such Gd-loaded apoferritin is quickly taken up by liver as this organ is rich of ferritin transporters. *In vitro* experiments upon incubation of this system in a primary culture of rat hepatocytes led to attain the minimum number of Gd necessary to MR visualization of a single cell. Thanks to its very high relaxivity, it was shown that cells can be visualized when they contain 10^7 Gd; i.e. more than one order of magnitude lower than the threshold defined using stem cells labeled with Gd-HPDO3A. The excellent properties shown by Gd-loaded apoferritin prompted further studies in order to assess its potential in targeting protocols. Geninatti Crich et al. first synthesized a derivative containing biotin residues on the outer surface, then targeted *via* avidin-NCAM (Neural Cell Adhesion Molecule) molecules that are over-expressed on the neoformed tumor endothelium (Fig. 20) [73]. The used procedure appears of general applicability provided from the availability of the biotinylated vector.

5.2. Gd-loaded lipoproteins

Other naturally occurring nanosized carriers that can be exploited for the delivery of MRI contrast agents are represented by lipoproteins.

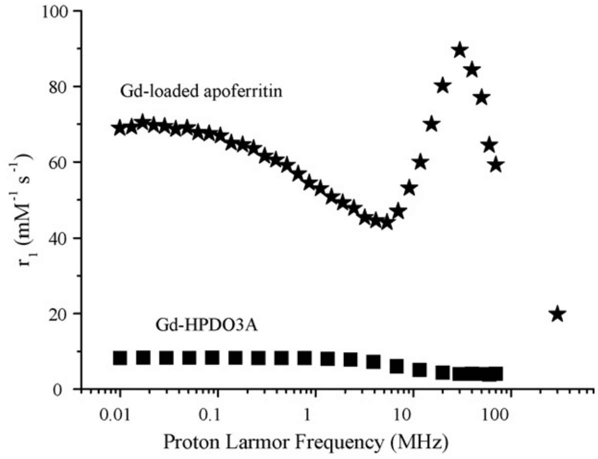

Fig. 19. NMRD profiles (298 K, pH 7) of Gd-HPDO3A free (squares) and entrapped in the apoferritin cavity (stars).

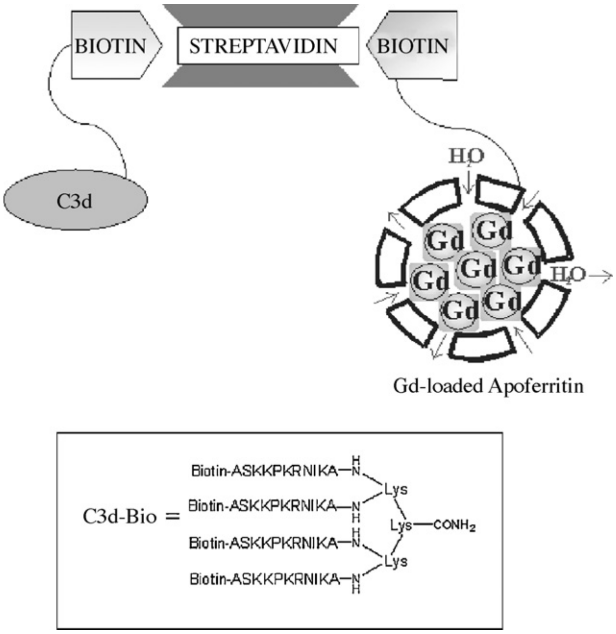

Fig. 20. Schematic view of the Gd-loaded apoferritin designed for targeting NCAM receptors. Adapted from ref. [73].

Among the different classes of lipoproteins, attention has been focused on Low Density Lipoproteins (LDL) and High Density Lipoproteins (HDL). The former systems are particles of *ca.* 25 nm diameter consisting of a high molecular weight protein (ApoB-100) that wraps around the lipidic core mainly made of cholesterol ester and stearic acid. The magnetic labeling of these particles has been attained by using amphiphilic paramagnetic complexes formed by one or two long aliphatic chain and an hydrophilic Gd(III) chelate. Such a system inserts its lipophilic moiety into the lipidic core of LDLs and exposes the Gd-containing cage to the aqueous phase. We found that it is possible to load up to 400 Gd-complexes per LDL particle (Fig. 21) by using Gd-AAZTA as MRI reporting unit, the relaxivity per particle being *ca.* 8800 $\mathrm{mM^{-1}\,s^{-1}}$. Such labeled LDLs maintain the targeting capabilities of the wild type precursors and show to accumulate at tumor cells thanks to an efficient internalization via the LDL receptors. This work nicely complements previous works reported by Glickson and co-workers, who pioneered the use of Gd-loaded LDL as specific tumor targeting agent [74]. HDL, although smaller than LDLs displays an analogous loading pattern and have been proposed as targeting agents for the MR visualization of atherosclerotic plaques [75].

6. Nanosized paramagnetic CEST agents

The new landscape of Molecular Imaging applications prompted the search for new paradigms in the design of MR-imaging reporters. A general insight deals with the exploitation of the frequency, the key parameter of the NMR phenomenon. The possibility of exploiting this parameter led to the development of agents based on peculiar properties of given heteronuclei (e.g. hyperpolarized noble gases atoms [76] or ^{13}C-containing molecules [77], as well as ^{19}F-based chemicals [78]). This approach has the advantage of dealing with images characterized by a zero background signal, but the attainment of sufficiently high sensitivity remains a quite challenging task. Therefore, the possibility of designing frequency-encoded MRI protocols based on the detection of the ^{1}H-water signal is still a very fascinating perspective.

The route to a new class of agents that conjugates frequency-encoding and water signal detection has its roots in the well established Magnetization Transfer (MT) MRI procedure, which relies on the transfer of saturated magnetization from tissutal mobile protons (water and labile protons from proteins) upon RF irradiation of their semi-solid like broad NMR absorption [79].

The use of exogenous probes, the so-called CEST (Chemical Exchange Saturation Transfer) agents, whose exchangeable protons resonances are characterized by a sharper absorption signal, introduces the possibility of selective RF irradiation [80,81]. Thus, one may design new protocols in which the contrast in a MR image is generated “at will” only if the proper frequency corresponding to the exchangeable protons of the added contrast agent is irradiated. Importantly, the new approach offers the unique possibility of detecting more than one agent in the same region [82,83], and, furthermore, the pre-contrast image can be recorded almost simultaneously to the post-contrast one as their acquisition simply differs from the on/off switch of the irradiating RF field.

Since CEST agents were discovered in 2000 [80], it was early realised that one of the main limiting factor for the *in vivo* application of such systems would have been represented by their relatively low sensitivity in comparison to the conventional Gd- and iron-based agents. Therefore, many efforts have been devoted to overcome this drawback.

Among the physico-chemical parameters controlling the efficiency of the saturation transfer (ST), the exchange rate of the mobile protons of the agent, k_{ex}, received much attention, either because it can be modulated by introducing suitable changes in the chemical structure of the probe, or because this parameter is usually dependent on variables like temperature or pH, that can make CEST agents potential responsive agents [84].

In principle, ST and k_{ex} are directly correlated, but this relationship is valid only until k_{ex} approaches the difference in the resonance frequency between the exchanging sites ($\Delta\omega$). In fact, when coalescence occurs, the mobile protons of the CEST agent are isochronous with the bulk water signal and the ST effect nul-

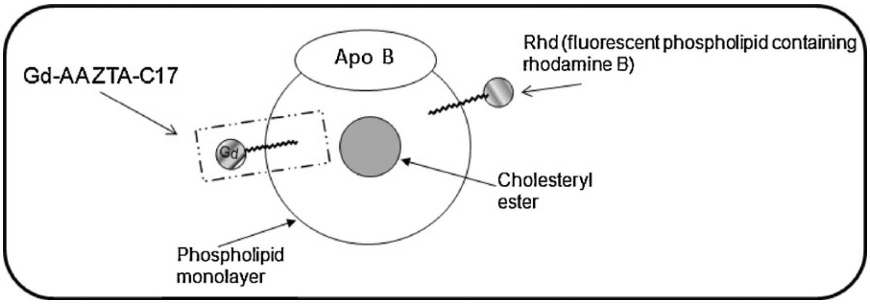

Fig. 21. Schematic representation of a LDL micelle labelled with a Gd(III)-based MRI agent and a fluorescent dye.

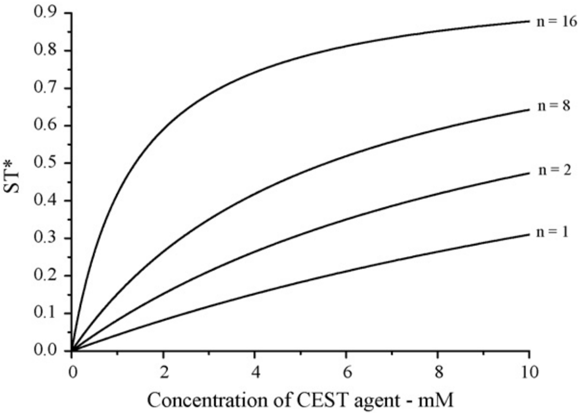

Fig. 22. Concentration dependence of ST according to the model reported in ref. [86] as a function of the number of equivalent mobile protons per CEST molecule (relevant parameters: $k_{ex} = 5000\ s^{-1}$, longitudinal relaxation rate of bulk water protons = $1\ s^{-1}$, irradiation time = 5 s).

lifies. The large $\Delta\omega$ values usually displayed by paramagnetic probes allows the exploitation of large k_{ex} values before the coalescence takes place, thus making the class of paramagnetic CEST agents the subject of intense scrutiny for this type of applications [85].

Theoretical considerations predict that the maximum ST efficiency is achieved when $k_{ex} = 2 \times \pi \times B_2$, where B_2 is the intensity of the saturation pulse. However, it is has to be recalled that for *in vivo* applications, B_2 value is limited by SAR (Specific Absorption Rate) constraints that, in turn, limit the possibility to enhance the ST efficiency through an increase of k_{ex}.

Another way to improve ST can be attained by increasing the number or equivalent or pseudo-equivalent (i.e. saturable by a single B_2 pulse) mobile protons belonging to the CEST agent. Fig. 22 reports a series of curves, simulated according to the simplified model developed by Zhou et al. [86], which highlights the noticeable role played by the number of saturated protons in defining the sensitivity of a CEST agent.

This prompted the search for highly sensitive CEST agents through the design of nanosized systems containing a high number of exchanging protons.

A first example based on this approach was proposed by our group in 2003 by exploiting the formation of a non-covalent supramolecolar adduct between a paramagnetic shift reagent (SR) and a macromolecular substrate acting as source of mobile protons [87].

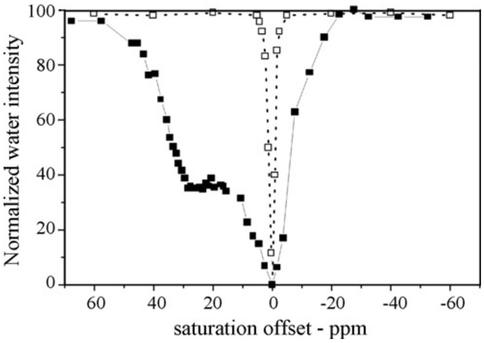

Fig. 23. Z-spectra of a solution of a 0.11 mM solution of poly-arginine alone (open squares) and in the presence of 2 mM of $[TmHDOTP]^{4-}$ (7 T, 312 K, pH 7.4, saturation scheme: 2 s single cw pulse, B_2 intensity 25 μT). The CEST peak at 30 ppm corresponds to the guanidine protons of the polymer shifted upon the interaction with the paramagnetic shift reagent. Adapted from ref. [84].

We used $[TmHDOTP]^{4-}$, a well known shift reagent for cations, and poly-arginine, a cationic polyaminoacid containing two different sets of potentially CEST-active mobile protons (the amide protons of the backbone, and the guanidine protons of the side chains). The Z-spectrum, reporting the intensity of the water signal as a function of the irradiation offset, of the polymer (0.11 mM) at pH 7.4 and 312 K (B_2 intensity 25 μT) does not show any ST (Fig. 23, open squares) because the exchange rate of the guanidine protons is too fast, whereas the ST detection from the amide protons is prevented by the large spillover effect caused by the relatively intense B_2 field.

By adding the paramagnetic shift reagent (18-fold molar excess), a supramolecolar adduct is formed and a CEST peak at about 30 ppm from free water appears in the Z-spectrum (Fig. 23, solid squares). It is likely that, in addition to the $\Delta\omega$ increase caused by the dipolar interaction with the shift reagent, also the exchange rate of the guanidine protons are affected by the tight binding with the metal complex (an association constant of about 3×10^4 was determined by relaxometric measurements).

The measurement of the ST effect in solutions containing different concentrations of the interacting species (maintaining the SR/Polyarg ratio of 18:1) demonstrates the noticeable sensitivity improvement attainable with this system (Fig. 24): in fact, a ST of 5% requires sub-mM concentrations of both polymer (1.7 μM) and shift reagent (30 μM).

A further breakthrough in the development of highly sensitive paramagnetic CEST agents was successively achieved by using

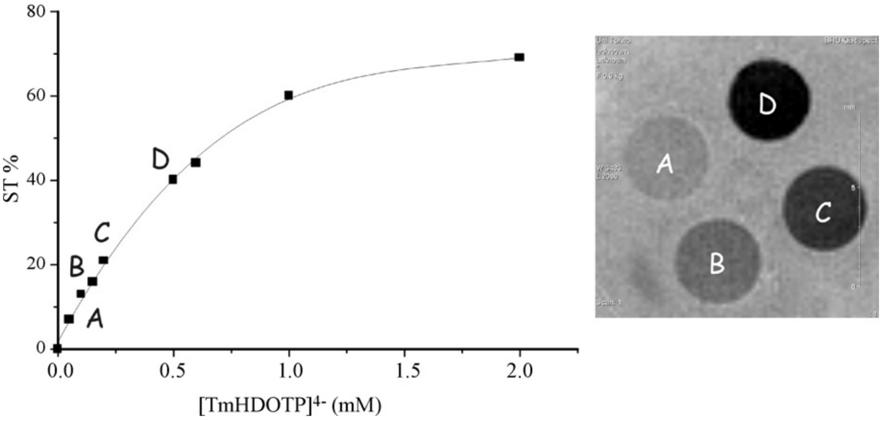

Fig. 24. Left: Concentration dependence of the saturation transfer for the $[TmHDOTP]^{4-}$/poly-arginine adduct (molar ratio 18:1) (7 T, 312 K, pH 7.4, saturation scheme: 2 s single cw pulse, B_2 intensity 25 μT). Right: MR-CEST difference image ($\nu_{30}-\nu_{-30}$). Adapted from ref. [84].

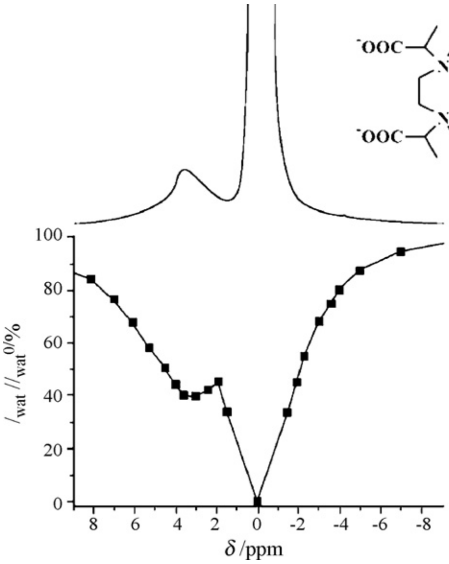

Fig. 25. NMR- (14.1 T) and Z- (7 T, saturation scheme: 3 s single cw pulse, B_2 intensity 12 μT) spectra of a suspension of liposomes entrapping [TmDOTMA]⁻ (showed in the inlet) at 312 K. The signal at 3.1 ppm from bulk water corresponds to the intraliposomal water protons. Adapted from ref. [88].

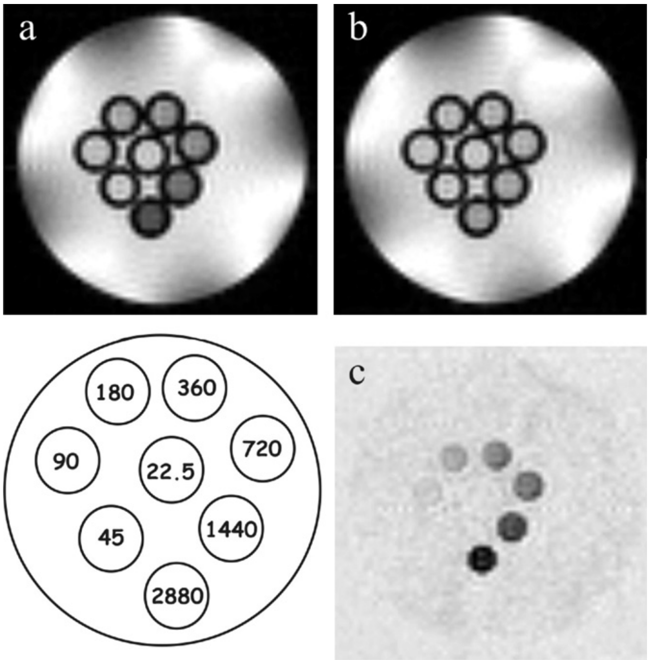

Fig. 26. MRI-CEST images of eight capillaries containing different concentrations of a LIPOCEST agent entrapping [TmDOTMA]⁻ (7 T, 312 K, saturation scheme: 120 sinc3 pulses 25 ms each, interpulse delay 10 μs, B_2 intensity 12 μT). (a) Image after saturation at 3.1 ppm. (b) Image after saturation at −3.1 ppm. (c) Image difference (a and b). Bottom left: concentrations of the agent in the capillaries. Adapted from ref. [88].

larger nanosystems like liposomes. Such biocompatible nanovesicles are optimal CEST platforms because their aqueous core contains an extraordinarily high number (10^7 to 10^9 depending on the liposome size) of water protons exchanging with the bulk solvent. The water protons inside and outside the cavity resonate at the same frequency ($\Delta\omega = 0$), but the entrapment of a hydrophilic paramagnetic shift reagent in the liposomal cavity produces a shift of the encapsulated water resonance, thus allowing the basic condition for a CEST probe ($\Delta\omega > k_{ex}$) to be fulfilled [88]. The best shift reagents have been found among paramagnetic metal complexes based on Ln(III) ions containing highly shifted and fast exchanging coordinated water molecule. The effect on the chemical shift of water protons induced by a Ln(III) complex is mainly dependent on the paramagnetism of the metal ion (expressed by the value of Bleaney's constant) and on the structure of the metal complex which determines the orientation of the metal bound water protons with respect to the magnetic axis of the complex. For instance, in axially symmetric macrocyclic Ln(III) complexes (e.g. [Ln-DOTMA]⁻) the coordinated water molecule is aligned along the magnetic axis and, consequently, the observed shift is very large [4].

In addition to the intrinsic efficiency of the SR, the chemical shift of the intraliposomal water protons is directly correlated to the concentration of the SR entrapped in the liposome. Fig. 25 (top) reports the ^{1}H NMR spectrum of a suspension of liposomes entrapping [TmDOTMA]⁻ at the concentration of 0.12 M.

The signal at about 4 ppm downfield from bulk water corresponds to the intraliposomal water protons. Accordingly, the Z-spectrum of the liposome suspension (Fig. 25, bottom) shows a CEST peak at the same frequency. The very large number of CEST-active water protons makes such agents (that we dubbed LIPOCEST) extremely sensitive. Fig. 26 reports a CEST difference image of a phantom of capillaries containing different liposome concentrations (indicated in nanomolar scale in the bottom left scheme) to show the dependence of the ST extent on the LIPOCEST concentration. The image indicates that a CEST contrast is still detectable in a solution containing *ca.* 100 pM of agent!

Furthermore, as the optimal B_2 intensity for maximizing the ST efficiency is related to the k_{ex} value, LIPOCEST agents do not require high saturation pulse intensity, because the typical exchange lifetime of intraliposomal water protons is in the milliseconds time scale.

For this reason, it is expected that the ST detection of LIPOCEST agents *in vivo* will not suffer from SAR constraints. However, it was soon recognized that a major drawback for the *in vivo* use of such nanosized agents is represented by the relatively small $\Delta\omega$ values (±4 ppm depending on the sign of the Bleaney's constant) that are determined by the intrinsic shifting ability of the SR and its maximum attainable intraliposomal concentration.

Therefore, efforts have been devoted to overcome this limitation [89]. It is known that a large contribution to the paramagnetic induced shift can arise from the occurrence of bulk magnetic susceptibility effects (BMS), which are operative when a paramagnetic agent is entrapped in non-spherical compartments that orient with respect to the external magnetic field [90,91]. To exploit the BMS contribution to further shift the intraliposomal water resonance, non-spherical liposomes have been produced by changing their original spherical shape upon their exposure to osmotic stress [92]. Fig. 27 reports the dependence of the chemical shift difference between intraliposomal and bulk water protons as a function of the osmolarity difference between the inner compartment (assumed to be equal to that one of the SR solution used for hydrating the thin lipidic film during the LIPOCEST preparation) and the solution in which the liposomes are dispersed.

Interestingly, when the liposomes are dispersed in a hyperosmotic fluid, the resonance of the intraliposomal water protons is significantly downfield shifted and the shift is independent of the sign of the Bleaney's constant of the Ln(III) ion, which, instead, defines the sign of the shift when the LIPOCESTs are dispersed in iso- or hypo-osmotic solutions.

The behaviour shown by the intraliposomal water resonance is fully consistent with the occurrence of a BMS contribution. In fact, for a given shape and orientation of the liposomes, the sign of the

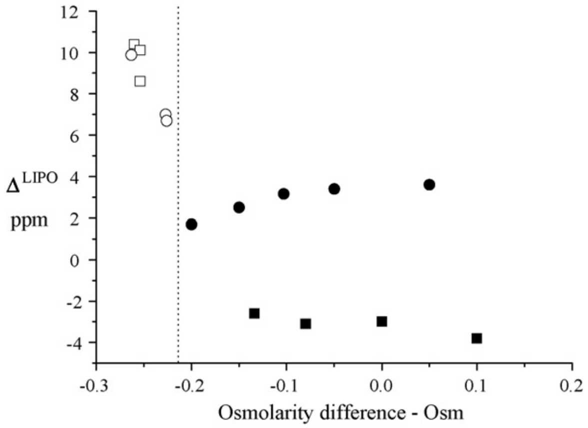

Fig. 27. Chemical shift of the intraliposomal water protons of several LIPOCESTs as a function of the osmolarity difference between the suspension medium (isotonic) and the hydration solution of the SR used for the liposomes preparation (squares: [Dy-HPDO3A], circles: [Tm-HPDO3A]).

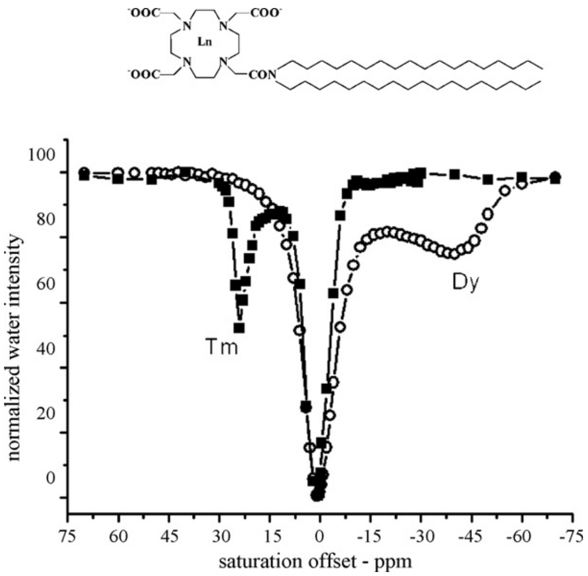

Fig. 28. Z-spectra (7 T, 312 K, saturation scheme: 2 s single cw pulse, B_2 intensity 6 μT) of two osmotically shrunken LIPOCEST agents encapsulating LnHPDO3A (Ln = Tm or Dy) and incorporating the amphiphilic SR showed in the inlet (Ln = Tm or Dy).

BMS shift is the same regardless of the Bleaney's constant of the Ln(III) ion.

A further progress has been achieved by enabling a better control of the orientation of the non-spherical liposomes. This task has been achieved by noting that the incorporation of paramagnetic amphiphilic Ln(III)-based complexes in bicelles (phospholipids-based binary bilayered micelles) strongly influences their orientation in the magnetic field according to the magnetic anisotropy of the metal complex [93,94]. On this basis, we investigated the CEST property of a new generation of LIPOCEST agents that contain a hydrophilic SR entrapped in the liposome cavity and an amphiphilic SR (complex **1**, Fig. 25) incorporated in the liposome membrane.

Fig. 28 shows the Z-spectra of two osmotically shrinked LIPOCEST agents of this type differing in the magnetic anisotropy of the encapsulated/incorporated SRs.

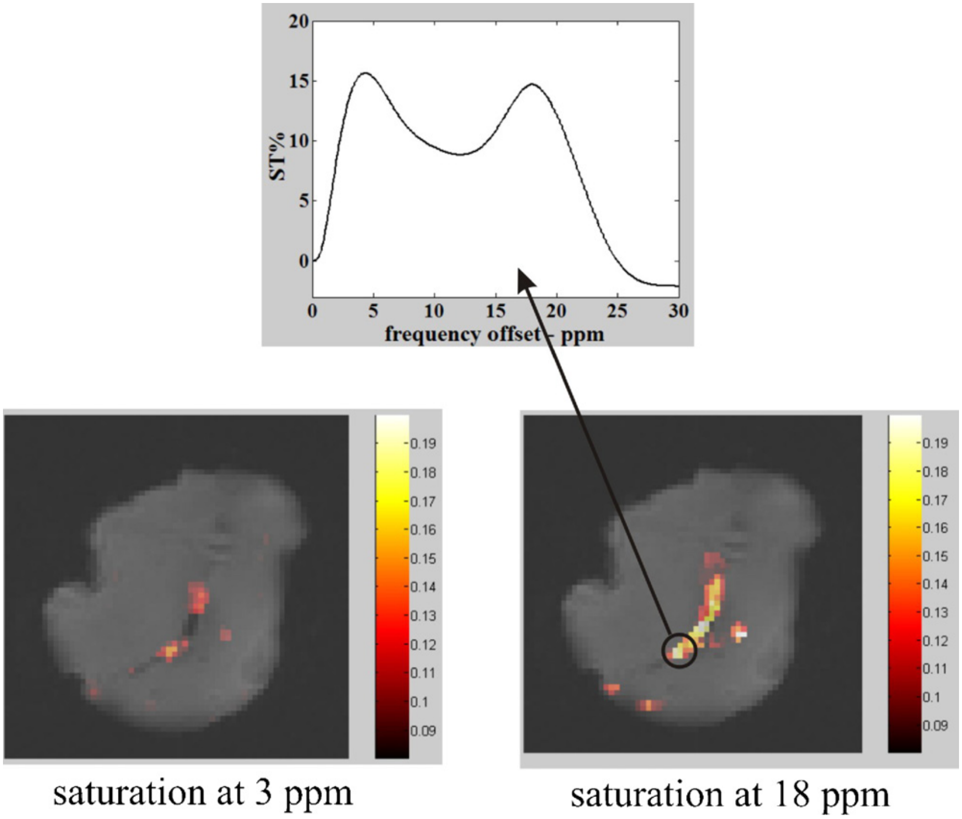

Fig. 29. ST maps at 3 ppm (left) and 18 ppm (right) superimposed to a Proton Density MR image of a bovine muscle injected with an aqueous suspension containing a spherical LIPOCEST ($\Delta\omega$ 3 ppm) and an osmotically shrunken LIPOCEST ($\Delta\omega$ 18 ppm) (7 T, 312 K). Saturation pulse intensity 3 μT. Top: ST profile of the selected region of interest. Adapted from ref. [83].

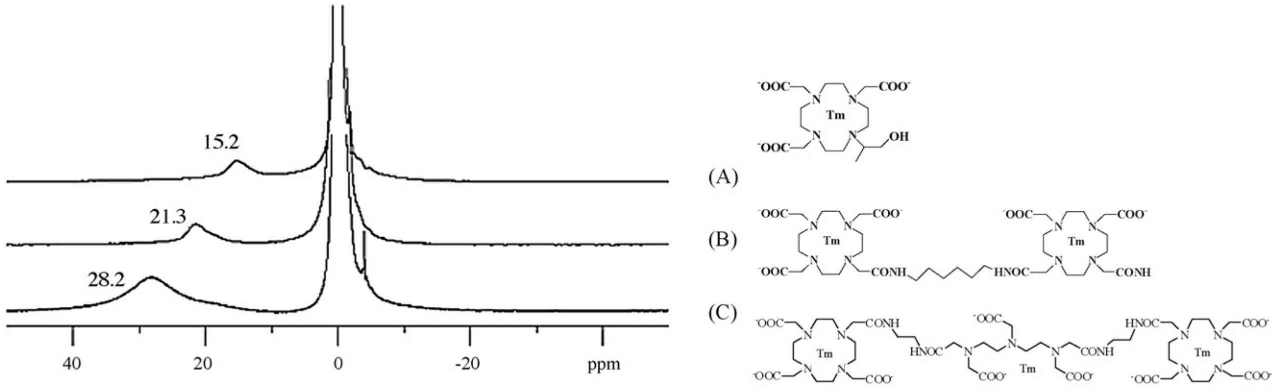

Fig. 30. ^{1}H NMR spectra (14.1 T, 298 K) of osmotically shrunken LIPOCESTs incorporating the amphiphilic Tm-complex reported in Figure X.7 and encapsulating a mono- (A), a bi- (B) and a tri-nuclear (C) Tm-based SR, respectively. Adapted from ref. [95].

The observed shifts for the intraliposomal water protons were considerably larger than those detected for the spherical LIPOCEST agents previously described. In addition, the sign of the induced shift is different: 18 ppm downfield for the Tm-based system and 45 ppm upfield for the Dy(III)-based agent, respectively. Clearly, the sign of the shift is controlled by the magnetic anisotropy of the incorporated SR.

The noticeable extension of the accessible saturation frequency values that can be achieved by the proper choice of the paramagnetic complexes will significantly improve the potential of such LIPOCEST probes. First of all, it is expected that the artefacts in the CEST-MR images caused by the asymmetry of the bulk water and/or the coil inhomogeneity will be reduced. Secondly, but not less important, this will facilitate the exploitation of the unique property of CEST agents, i.e. the visualization of different LIPOCEST probes in the same region of interest.

This latter concept is nicely demonstrated in Fig. 29 that reports the first example of detection of two LIPOCEST agents (one spherical and one osmotically shrunken) co-injected in a bovine muscle [83].

Another strategy in order to further increase the $\Delta\omega$ value for LIPOCEST agents has been very recently proposed [95]. The resonance frequency of the intraliposomal water protons is directly correlated to the concentration of the encapsulated SR in the aqueous core of the vesicle, and, therefore, the entrapment of a higher number of paramagnetic centres in the aqueous core should ensure larger shifts. Since the intraliposomal SR concentration is primarily limited by osmotic forces, the encapsulation of polynuclear neutral Ln(III) complexes should be highly beneficial. This concept is clearly showed in Fig. 30, which compares the chemical shift of the intraliposomal water protons in three osmotically shrunken LIPOCESTs encapsulating neutral Tm-based SRs of different nuclearity.

Finally, the exploitation of a BMS shift in non-spherical liposomes makes also possible the design of LIPOCEST agents containing a Gd(III) complex [96]. The very intriguing peculiarity of such agents is that they can act as T_1, T_2 and CEST agents at the same time! Fig. 31 demonstrates the potential of this novel class of multi-contrast modality agents on a phantom containing a solution of a LIPOCEST entrapping the clinically approved MRI agent ProHance^{TM}.

In addition to the great sensitivity enhancement, the use of nanosized CEST agents may be extremely advantageous also for designing responsive and targeting probes.

A nice example of the former systems has been very recently published by Pikkemaat et al. [97], who investigated the pH-responsiveness of a series of dendrimer-based CEST agents. The authors used different generations of polypropylene imine dendrimers (G1 and G3) whose terminal nitrogens were fully conjugated with pH responsive PARACEST moieties (based on the well performing Yb-DOTAM coordination cage [98]). In addition to the expected sensitivity improvement (about 20 μM with a ST threshold of 5%), the larger system (G3, containing more than 100 amide protons per dendrimer) displayed a pH-responsiveness properly tuned at the physio-pathological range of interest (Fig. 32).

Sherry's group at Dallas is actively searching for metabolic imaging reporters based on CEST effect [99,100]. It is likely that several of the systems they have developed would find a definitely strong sensitivity improvement when they will be transferred on nanosized scaffolds.

As far as the targeting probes is concerned, an interesting example was recently reported by Winter et al., who used perfluorocarbon nanoparticles as platform for binding amphiphilic Eu(III)-based PARACEST agents (again based on the well performing DOTA tetraamide coordination cage), and monoclonal antifibrin antibodies via biotin–avidin linkage [101]. This fibrin-targeted PARACEST nanoparticles displayed high sensitivity (owing to the high number of metal complexes bound to the nanoparticle) upon

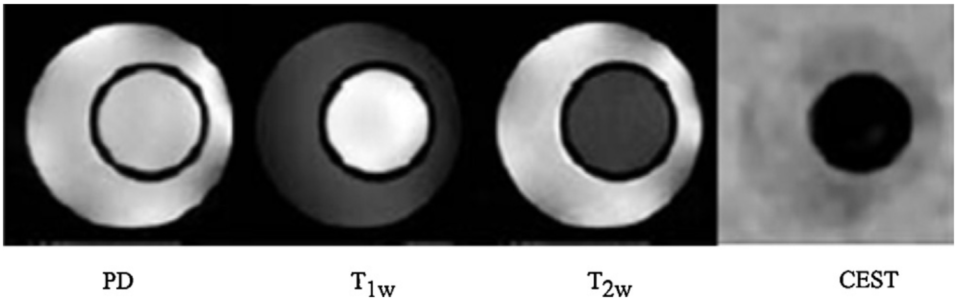

Fig. 31. MR images (7 T, 312 K) of a capillary, dipped into neat water, containing a suspension of an osmotically shrunken Gd-based liposome. From left to right: Proton density image, T_{1w} image, T_{2w} image, and CEST difference image (ν_7–ν_{-7}, saturation scheme: 2 s single cw pulse, B_2 intensity 6 μT). Adapted from ref. [96].

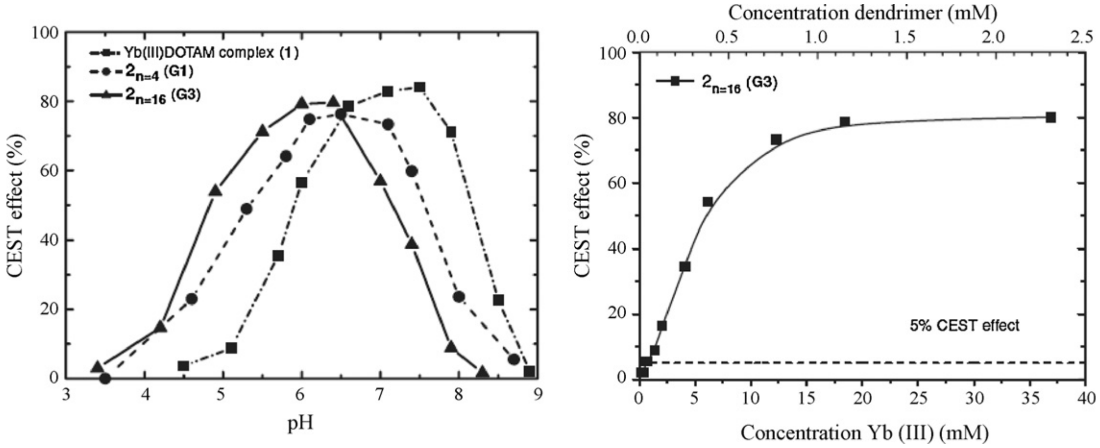

Fig. 32. Left: pH dependence of ST efficiency (at 13.5 ppm) for Yb-DOTAM (30 mM), G1 (7.4 mM) and G3 (1.9 mM) PARACEST-based dendrimers (7 T, 310 K, irradiation time 2 s, B_2 intensity 22 μT). Right: Concentration dependence of ST efficiency (at 13.5 ppm) for G3 PARACEST-based dendrimer (7 T, 310 K, pH 6.3, irradiation time 2 s, B_2 intensity 22 μT). Adapted from ref. [98].

saturation at 52 ppm, corresponding to the resonance frequency of the Eu-coordinated water protons. This targeted nanosized construct is able to visualize specifically the outer surface of artificial plasma clots, as shown in Fig. 33.

7. Concluding remarks

The low sensitivity of the MRI methodology was thought to strongly limit the involvement of this modality in the development of the Molecular Imaging field [102]. However, a number of achievements in pre-clinical studies indicate that MRI still may have a role in this challenging field. On one hand there is the outstanding development of hyperpolarized molecules that tackles the sensitivity problem at its roots providing innovative routes for the visualization of cellular metabolism [103].

Next, good progresses have been made on the route of entrapping small-sized MRI probes into the diseased cells thanks to targeting transporters that are over-expressed in the presence of a given pathology [104]. However, the most general route to overcome sensitivity problems relies on the availability of nanosized carriers that can deliver huge payloads of imaging reporters at the targeting site. As shown in Fig. 34, chemistry of auto-assembled lipophilic systems may offer a number of possible solutions only part explored.

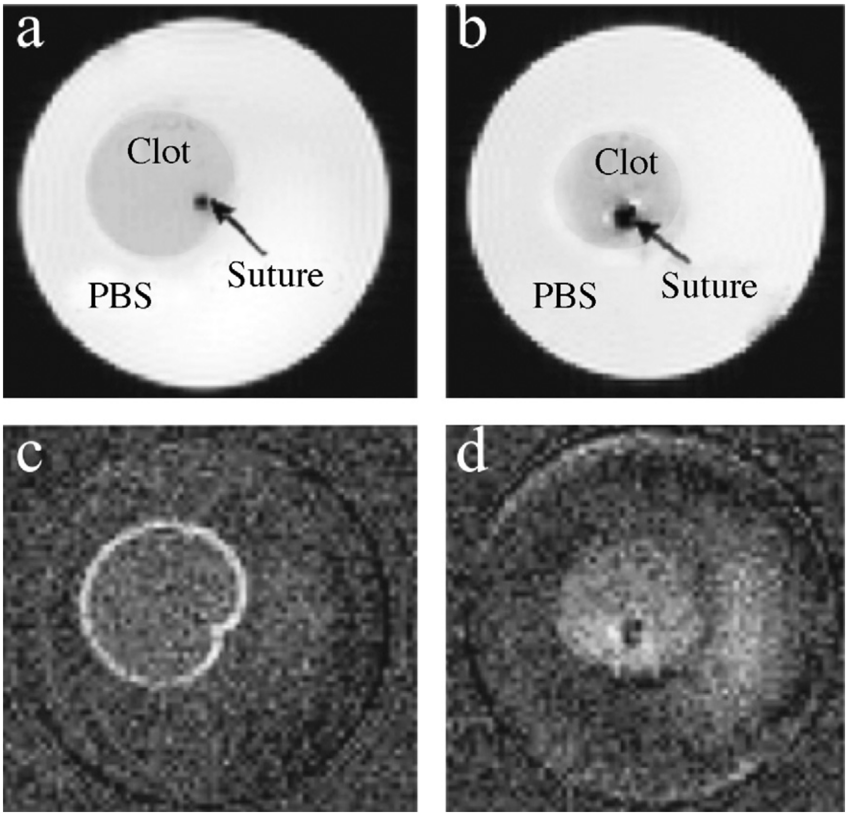

Fig. 33. MR images of human plasma clots. (a and b) After saturation at −52 ppm. (c and d) CEST difference images ($\nu_{-52}-\nu_{52}$). (a and c) Clot treated with the fibrin-targeted PARACEST nanoparticles. (b and d) Control. Adapted from ref. [101].

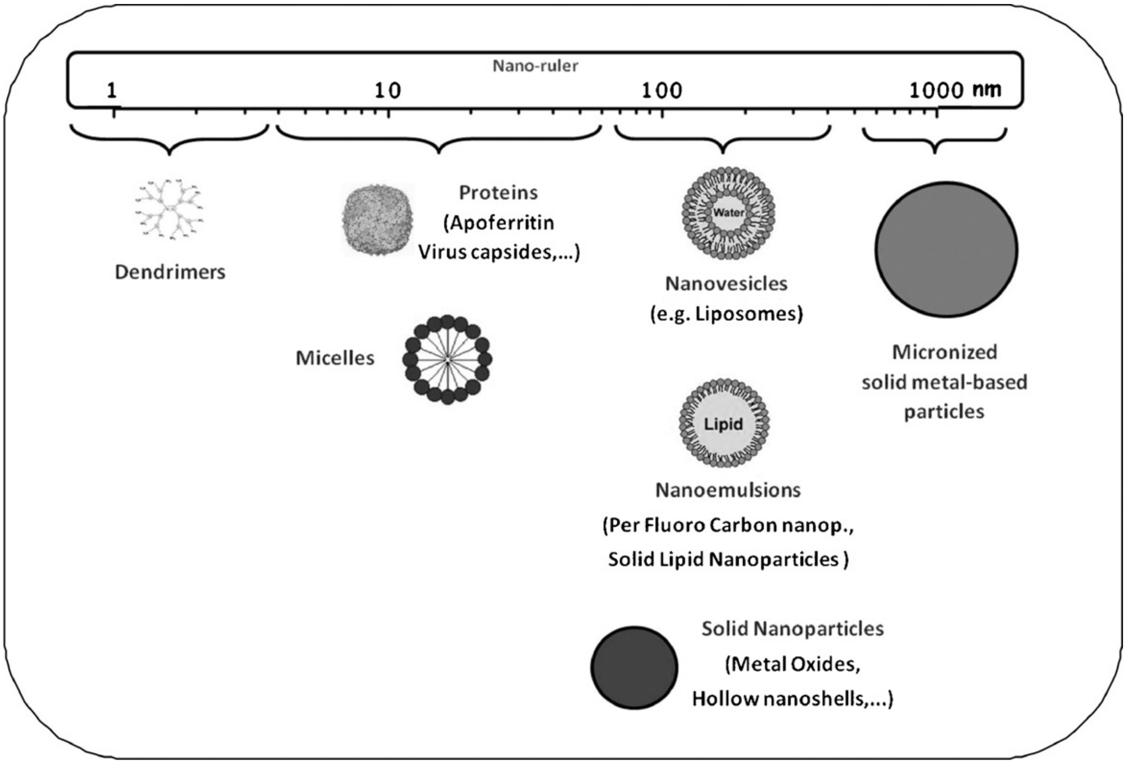

Fig. 34. Some of the nanosized carriers considered for designing highly efficient MRI agents for Molecular Imaging applications.

Though not included in the present survey, there is the important contribution by Wickline and co-workers in the field of microemulsions. They showed that such nanoparticles can be loaded up with 10^5 Gd(III) ions, thus generating MRI probes that visualize endothelial targets at very low concentration [105]. Recently, they added a new valuable contribution to the use of these particles by measuring the quantitative ^{19}F MR signal present as major component of the microemulsion [106]. From the ^{19}F determination, it is possible to assess the actual *in vivo* relaxivity of the Gd(III)-complexes.

Herein, we have shown that several auto-assembled systems, when loaded with Gd(III)-complexes, display a sensitivity sufficient to overcome the threshold for the MRI visualization. Moreover, upon tackling the sensitivity issues, it has been shown that the peculiar structures of such nanosized systems may be exploited to develop novel classes of contrast agents such as in the case of LIPOCEST. All together, the achievements made in the use of these nanocarriers in MRI applications represent the basis for the development of the field of imaging the drug delivery process. The superb anatomical resolution provided by MR images together with the availability of targeting and responsive agents will allow the clinician to pursue the task of visualizing the delivery of drugs at the diseased region and, even more important, to monitor the therapeutic output in real time.

Acknowledgements

Economic and scientific support from MIUR (FIRB RBNE03-PX83_006, FIRB RBIP06293N, and PRIN 2005039914 projects), EC-FP6-projects DiMI (LSHB-CT-2005-512146), EMIL (LSHC-CT-2004-503569), MEDITRANS (Targeted Delivery of Nanomedicine: NMP4-CT-2006-026668), and EU-COST D38 Action is gratefully acknowledged.

References

[1] R. Weissleder, U. Mahmood, Radiology 219 (2001) 316.
[2] S. Aime, C. Cabella, S. Colombatto, S. Geninatti Crich, E. Gianolio, F. Maggioni, JMRI 16 (2002) 394.
[3] C.H. Cunningham, T. Arai, P.C. Yang, M.V. McConnell, J.M. Pauly, S.M. Conolly, Magn. Reson. Med. 53 (2005) 999.
[4] S. Aime, S. Geninatti Crich, E. Gianolio, G.B. Giovenzana, L. Tei, E. Terreno, Coord. Chem. Rev. 250 (2006) 1562.
[5] R.N. Muller, L. Vander Elst, A. Roch, J.A. Peters, E. Csajbok, P. Gillis, Y. Gossuin, Adv. Inorg. Chem. 57 (2005) 239.
[6] C. Corot, P. Robert, J.M. Idee, M. Port, Adv. Drug Deliv. Rev. 58 (2006) 1471.
[7] G. Schumann Giamperi, Invest. Radiol. 28 (1993) 753.
[8] J.W.M. Bulte, J. Magn. Magn. Mater. 289 (2005) 423.
[9] R.D.O. Engberink, S.M.A. van der Pol, E.A. Dopp, E.L.A. Blezer, Radiology 243 (2007) 467.
[10] A. Saleh, M. Schroeter, C. Jonkmanns, H.-P. Hartung, U. Modder, S. Jander, Brain 127 (2004) 1670.
[11] V. Dousset, B. Brochet, M.S.A. Deloire, L. Lagoarde, B. Barroso, J.-M. Caille, K.G. Petri, Am. J. Neuroradiol. 27 (2006) 1000.
[12] U. Himmelreich, S. Aime, T. Hieronymus, C. Justicia, F. Uggeri, M. Zenke, M. Hoehn, Neuroimage 32 (2006) 1142.
[13] W.J.M. Mulder, G.J. Strijkers, G.A.F. van Tilborg, A.W. Griffioen, K. Nicolay, NMR Biomed. 19 (2006) 142.
[14] G.M. Nicolle, E. Toth, K.P. Eisenwiener, H.R. Maecke, A.E. Merbach, J. Biol. Inorg. Chem. 7 (2002) 757.
[15] G.M. Nicolle, L. Helm, A.E. Merbach, Magn. Reson. Chem. 41 (2003) 794.
[16] S. Torres, J.A. Martins, J.P. Andrè, C.F.G.C. Geraldes, A.E. Merbach, E. Toth, Chem. Eur. J. 12 (2006) 940.
[17] R. Hovland, C. Glogard, A.J. Aasen, J. Klaveness, Org. Biomol. Chem. 1 (2003) 644.
[18] E. Gianolio, G.B. Giovenzana, D. Longo, I. Longo, I. Menegotto, S. Aime, Chem. Eur. J. 13 (2007) 5785.
[19] A. Accardo, D. Tesauro, P. Roscigno, E. Gianolio, L. Padano, G. D'Errico, C. Pedone, G. Morelli, J. Am. Chem. Soc. 126 (2004) 3097.
[20] A. Accardo, D. Tesauro, G. Morelli, E. Gianolio, S. Aime, M. Vaccaio, G. Mangiapia, L. Padano, K. Schillen, J. Biol. Inorg. Chem. 12 (2007) 267.
[21] M. Vaccaro, G. Mangiapia, L. Padano, E. Gianolio, A. Accardo, D. Tesauro, G. Morelli, Chemphyschem 17 (2007) 2526.
[22] G. Lipari, A. Szabo, J. Am. Chem. Soc. 104 (1982) 4546.
[23] G. Lipari, A. Szabo, J. Am. Chem. Soc. 104 (1982) 4559.
[24] E. Gianolio, G.B. Giovenzana, A. Ciampa, S. Lanzardo, D. Imperio, S. Aime, ChemMedChem 3 (2008) 60.

[25] H.J. Raatschen, R. Swain, D.M. Shames, Y. Fu, Z. Boyd, M.L. Zierhut, M.F. Wendland, B. Misselwitz, H.J. Weinmann, K.J. Wolf, R.C. Brasch, Contrast Med. Mol. Imaging 1 (2006) 113.
[26] M.J. Lipinski, V. Amirbekian, J.C. Frias, J.G.S. Aguinaldo, V. Mani, K.C. Briley-Saebo, V. Fuster, J.T. Fallon, E.A. Fischer, Z. Fayad, Magn. Reson. Med. 56 (2006) 601.
[27] V. Amirbekian, M.J. Lipinski, K.C. Briley-Saebo, S. Amirbekian, J.G.S. Aguinaldo, D.B. Weinreb, E. Vcic, J.C. Frias, F. Hyafil, V. Mani, E.A. Fisher, Z.A. Fayad, PNAS 104 (2007) 961.
[28] J. Barkhausen, W. Ebert, C. Heyer, J.F. Debatin, H.J. Weinmann, Circulation 108 (2003) 605.
[29] A.D. Bangham, M.M. Standish, J.C. Watkins, J. Mol. Biol. 13 (1965) 238.
[30] S.H. Koenig, R.D. Brown III, R. Kurland, S. Ohki, Magn. Reson. Med. 7 (1988) 133.
[31] C. Tilcock, E. Unger, P. Cullis, P. MacDougall, Radiology 171 (1989) 77.
[32] V.J. Caride, H.D. Sostman, R.J. Winchell, J.C. Gore, Magn. Reson. Imaging 2 (1984) 107.
[33] S.L. Fossheim, K.A. Il'asov, J. Hennig, A. Bjornerud, Acad. Radiol. 7 (2000) 1107.
[34] S.L. Fossheim, A.K. Fahlvik, J. Klaveness, R.N. Muller, Magn. Reson. Imaging 17 (1999) 83.
[35] E.C. Unger, T. Winokur, P. MacDougall, J. Rosenblum, M. Clair, R. Gatenby, C. Tilcock, Radiology 171 (1989) 81.
[36] M.R. Niesman, G.C. Bacic, S.M. Wright, H.J. Swartz, R.L. Magin, Invest. Radiol. 25 (1990) 545.
[37] K.E. Lokling, R. Skurtveit, K. Dyrstad, J. Klaveness, S.L. Fossheim, Int. J. Pharm. 274 (2004) 75.
[38] K.E. Lokling, S.L. Fossheim, J. Klaveness, R. Skurtveit, J. Controlled Release 98 (2004) 87.
[39] G. Kong, M.W. Dewhirst, Int. J. Hyperthermia 15 (1999) 345.
[40] L. Frich, A. Bjornerud, S. Fossheim, T. Tillung, I. Gladhaug, Magn. Reson. Med. 52 (2004) 1302.
[41] L.H. Lindner, H.M. Reinl, M. Schlemmer, R. Stahl, M. Peller, Int. J. Hyperthermia 21 (2005) 575.
[42] E. Terreno, A. Bert, W. Dastrù, A. Sanino, S. Aime, Proc. Joint Annual Meeting ISMRM-ESMRMB, Berlin, Germany, 2007, p. 252.
[43] B.L. Viglianti, S.A. Abraham, C.R. Michelich, P.S. Yarmolenko, J.R. MacFall, M.B. Bally, M.W. Dewhirst, Magn. Reson. Med. 51 (2004) 1153.
[44] C. Tilcock, Q.F. Ahkong, S.H. Koenig, R.D. Brown III, M. Davis, G. Kabalka, Magn. Reson. Med. 27 (1992) 44.
[45] C. Glogard, G. Stensrud, R. Hovland, S.L. Fossheim, J. Klaveness, Int. J. Pharm. 233 (2002) 131.
[46] S. Aime, M. Botta, M. Fasano, E. Terreno, Acc. Chem. Res. 32 (1999) 941.
[47] C. Cabella, S. Geninatti Crich, D. Corpillo, A. Barge, C. Ghirelli, E. Bruno, V. Lorusso, F. Uggeri, S. Aime, Contr. Media Mol. Imaging 1 (2006) 23.
[48] I. Bertini, F. Bianchini, L. Calorini, S. Colagrande, M. Fragrai, A. Franchi, O. Gallo, C. Gavazzi, C. Luchinat, Magn. Res. Med. 52 (2004) 669.
[49] G.J. Strijkers, W.J.M. Mulder, R.B. Heeswijk, P.M. Frederik, P. Bomans, P.C. Magusin, K. Nicolay, MAGMA 18 (2005) 186.
[50] L. Tei, S. Geninatti Crich, B. Bussolati, A. Ciampa, C. Grange, D. Alberti, S. Lanzardo, G. Camussi, S. Aime, Proc. Joint Annual Meeting ISMRM-ESMRMB, Berlin, Germany, 2007, p. 256.
[51] D.A. Sipkins, D.A. Cheresh, M.R. Kazemi, L.M. Nevin, M.D. Bednarski, K.C. Li, Nat. Med. 4 (1998) 623.
[52] W.J. Mulder, G.J. Strijkers, J.W. Habets, E.J. Bleeker, D.W. van der Schaft, G. Storm, G.A. Koning, A.W. Griffionen, K. Nicolay, FASEB J. 19 (2005) 2008.
[53] W.J.M. Mulder, K. Douma, G.A. Koning, M.A. van Zandvoort, E. Lutgens, M.J. Daemen, K. Nicolay, G.J. Strijkers, Magn. Reson. Med. 55 (2006) 1170.
[54] V.S. Trubetskoy, J.A. Cannillo, A. Milshtein, G.L. Wolf, V.P. Torchilin, Magn. Reson. Imaging 13 (1995) 31.
[55] D.A. Sipkins, K. Gijbels, F.D. Tropper, M. Bednarski, K.C. Li, L. Steinman, J. Neuroimmunol. 104 (2000) 1.
[56] W.J. Chu, T. Simor, G.A. Elgavish, NMR Biomed. 10 (1997) 87.
[57] W.J. Mulder, D.W. van der Schaft, P.A.I. Hautvast, G.J. Strijkers, G.A. Koning, G. Storm, K.H. Mayo, A.W. Griffionen, K. Nicolay, FASEB J. 21 (2007) 378.
[58] W.J. Mulder, A.W. Griffionen, G.J. Strijkers, D.P. Cormode, K. Nicolay, Z.A. Fayad, Nanomedicine 2 (2007) 307.
[59] B.R. Rosen, J.W. Belliveau, H.J. Aronen, D. Kennedy, B.R. Buchbinder, A. Fischman, M. Gruber, J. Glas, R.M. Weisskoff, M.S. Cohen, F.H. Hochberg, T.J. Brady, Magn. Reson. Med. 22 (1991) 293.
[60] L.M. Hamberg, R. MacFarlane, E. Tasdemiroglu, P. Boccalini, G.J. Hunter, J.W. Belliveau, M.A. Moskowitz, B.R. Rosen, Stroke 24 (1993) 444.
[61] S.L. Fossheim, K.E. Kellar, A.H. Fahlvik, J. Klaveness, Magn. Reson. Imaging (1997) 193.
[62] E. Terreno, C. Cabella, C. Carrera, D. Delli Castelli, S. Lanzardo, R. Mazzon, S. Rollet, M. Visigalli, S. Aime, Proc. Joint Annual Meeting ISMRM-ESMRMB, Berlin, Germany, 2007, p. 248.
[63] J.W. Bulte, M. De Cuyper, Methods Enzymol. 373 (2003) 175.
[64] M. Babincova, V. Altanerova, M. Lampert, C. Altaner, E. Machova, M. Sramka, P. Babinec, Z. Naturforsch. C 55 (2000) 278.
[65] M. Babincova, D. Leszczynska, P. Sourivong, P. Babinec, J. Leszczynski, Med. Hypotheses 62 (2004) 375.
[66] A. Ito, M. Shinkai, H. Honda, T. Kobayashi, J. Biosci. Bioeng. 100 (2005) 1.
[67] M.S. Martina, J.P. Fortin, C. Menager, O. Clement, G. Barratt, C. Grabielle-Madelmont, F. Gazeau, V. Cabuil, S. Lesieur, J. Am. Chem. Soc. 127 (2005) 10676.
[68] J.W. Bulte, M. De Cuyper, D. Despres, J.A. Franck, J. Magn. Reson. Imaging 9 (1999) 329.
[69] J.P. Fortin-Ripoche, M.S. Martina, F. Gazeau, C. Menager, C. Wilhelm, J.C. Bacri, S. Lesieur, O. Clement, Radiology 239 (2006) 415.
[70] S. Aime, L. Frullano, S. Geninatti Crich, Angew. Chem. Int. Ed. 41 (2002) 1017.
[71] B. Webb, J. Frame, Z. Zhao, M.L. Lee, G.D. Watt, Arch. Biochem. Biophys. 309 (1994) 178.
[72] O. Vasalatiy, P. Zhao, S. Zhang, S. Aime, A.D. Sherry, Contrast Med. Mol Imaging 1 (2006) 10.
[73] S. Geninatti Crich, B. Bussolati, L. Tei, C. Grange, G. Esposito, S. Lanzardo, G. Camussi, S. Aime, Cancer Res. 66 (2006) 9196.
[74] I.R. Corbin, H. Li, J. Chen, S. Lund-Katz, R. Zhou, J.D. Glickson, G. Zheng, Neoplasia 8 (2006) 488.
[75] J.C. Frias, K.J. Williams, E.A. Fisher, Z.A. Fayad, J. Am. Chem. Soc. 126 (2004) 16316.
[76] H. Kauczor, R. Surkau, T. Roberts, Eur. Radiol. 8 (1998) 820.
[77] K. Golman, J.S. Petterson, Acad. Radiol. 13 (2006) 932.
[78] J.X. Yu, V.D. Kodibagkar, W. Cui, R.P. Mason, Curr. Med. Chem. 12 (2005) 819.
[79] R.M. Henkelman, G.J. Stanizs, S.J. Graham, NMR Biomed. 14 (2001) 57.
[80] K.M. Ward, A.H. Aletras, R.S. Balaban, J. Magn. Res. 143 (2000) 79.
[81] J. Zhou, P.C.M. van Zijl, Prog. NMR Spectr. 48 (2006) 109.
[82] S. Aime, C. Carrera, D. Delli Castelli, S. Geninatti Crich, E. Terreno, Angew. Chem. Int. Ed. 44 (2005) 1813.
[83] E. Terreno, D. Delli Castelli, S. Rollet, J. Stancanello, E. Violante, S. Aime, Contrast Med. Mol. Imaging 3 (2008) 38.
[84] M. Woods, D.E. Woessner, A.D. Sherry, Chem. Soc. Rev. 35 (2006) 500.
[85] S. Zhang, M. Merritt, D.E. Woessner, R.E. Lenkinski, A.D. Sherry, Acc. Chem. Res. 36 (2003) 783.
[86] J. Zhou, D.A. Wilson, P.Z. Sun, J.A. Klaus, P.C.M. van Zijl, Magn. Reson. Med. 51 (2004) 945.
[87] S. Aime, D. Delli Castelli, E. Terreno, Angew. Chem. Int. Ed. 42 (2003) 4527.
[88] S. Aime, D. Delli Castelli, E. Terreno, Angew. Chem. Int. Ed. 44 (2005) 5513.
[89] E. Terreno, C. Cabella, C. Carrera, D. Delli Castelli, R. Mazzon, S. Rollet, J. Stancanello, M. Visigalli, S. Aime, Angew. Chem. Int. Ed. 46 (2007) 966.
[90] S.C.K. Chu, Y. Xu, J.A. Balschi, C.S. Springer Jr., Magn. Reson. Med. 13 (1990) 239.
[91] P.W. Kuchel, B.E. Chapman, W.A. Bubb, P.E. Hansen, C.J. Durrant, M.P. Hertzberg, Concepts Magn. Res. A 18A (2003) 56.
[92] J. Pencer, G.F. White, F.R. Hallett, Biophys. J. 81 (2001) 2716.
[93] R.S. Prosser, S.A. Hunt, J.A. Di Natale, R.R. Vold, J. Am. Chem. Soc. 118 (1996) 269.
[94] R.S. Prosser, H. Bryant, R.G. Bryant, R.R. Vold, J. Magn. Res. 141 (1999) 256.
[95] E. Terreno, A. Barge, L. Beltrami, G. Cravotto, D. Delli Castelli, F. Fedeli, B. Jebasingh, S. Aime, Chem. Commun. (2008) 600.
[96] S. Aime, D. Delli Castelli, D. Lawson, E. Terreno, J. Am. Chem. Soc. 129 (2007) 2430.
[97] J.A. Pikkemaat, R.T. Wegh, R. Lamerichs, R.A. van de Molengraf, S. Langereis, D. Burdinski, A.Y.F. Raymond, H.M. Janssen, B.F.M. de Waal, N.P. Willard, E.W. Mejer, H. Grull, Contrast Med. Mol. Imaging 2 (2007) 229.
[98] S. Zhang, L. Michaudet, S. Burgess, A.D. Sherry, Angew. Chem. Int. Ed. 41 (2002) 1919.
[99] S. Zhang, R. Trokowski, A.D. Sherry, J. Am. Chem. Soc. 125 (2003) 15288.
[100] R. Trokowski, J. Ren, F.K. Kalman, A.D. Sherry, Angew. Chem. Int. Ed. 44 (2005) 6920.
[101] P.M. Winter, K. Cai, J. Chen, C.R. Adair, G.E. Kiefer, P.S. Athey, P.J. Gaffney, C.E. Buff, J.D. Robertson, S.D. Caruthers, S.A. Wickline, G.M. Lanza, Magn. Reson. Med. 56 (2006) 1384.
[102] A.D. Nunn, K.E. Linder, M.F. Tweedle, Q. J. Nucl. Med. 41 (1997) 155.
[103] K. Golman, R. in't Zandt, M. Lerche, R. Pehrson, J.H. Ardenkjaer-Larsen, Cancer Res. 66 (2006) 10855.
[104] S. Geninatti Crich, C. Cabella, A. Barge, S. Belfiore, C. Ghirelli, L. Lattuada, S. Lanzardo, A. Mortillaro, L. Tei, M. Visigalli, G. Forni, S. Aime, J. Med. Chem. 49 (2006) 4926.
[105] A.M. Morawski, P.M. Winter, K.C. Crowder, S.D. Caruthers, R.W. Fuhrhop, M.J. Scott, J. David Robertson, D.R. Abendschein, G.M. Lanza, S.A. Wickline, Magn. Reson. Med. 51 (2004) 480.
[106] A.M. Morawski, P.M. Winter, X. Yu, R.W. Fuhrhop, M.J. Scott, F. Hockett, J. David Robertson, P.J. Gaffney, G.M. Lanza, S.A. Wickline, Magn. Reson. Med. 52 (2004) 1255.